Natural Polyisoprene Composites and Their Electronic Applications

Deepalekshmi Ponnamma, Kishor Kumar Sadasivuni, K.T. Varughese, Sabu Thomas and Mariam Al-Ali AlMa'adeed

Abstract Rubber-based composites have been recognized as efficient materials for the fabrication of technologically important products. Various particles are successfully incorporated into cis-polyisoprene or natural rubber (NR) in recent years both in solution and in melt forms. Potential electronic applications of such composites specifically containing carbon nanotubes, graphene, graphene-like structures, fibers, metallic fillers, and inorganic fillers have been realized in this article. Advanced performances of NR composites obtained via different methods are compared with those of the neat polymer. Special attention is paid to the structural changes occurring in the matrix under the influence of fillers. Other issues regarding the technology limitations, research challenges, and future trends are also discussed. The main objective of this review is threefold: (1) to present the latest electronic applications of NR composite technology and development, (2) to describe the need for fundamental research in this field, and (3) to outline major challenges in rubber composite preparation. At first an overview of NR composites, then their preparation methods, and thereafter their applications are described. In short, other than summarizing different classes of particles filled NR composites and their applications, this review highlights different ways to create smaller, cheaper, lighter, and faster devices based on such materials. The developed materials are highly useful in the fields of electronics and diffusion as well as in the marine and transport industries.

Keywords Rubber · Actuator · Sensor · Electronics · Microwave absorbers · Supercapacitors

D. Ponnamma (✉) · K.K. Sadasivuni · M.A.-A. AlMa'adeed
Center for Advanced Materials, Qatar University, P.O. Box 2713, Doha, Qatar
e-mail: lekshmi_deepa@yahoo.com

K.T. Varughese
Polymer Laboratory, Dielectric Materials Division, Central Power Research Institute, Bangalore 560080, India

D. Ponnamma et al. (eds.), *Flexible and Stretchable Electronic Composites*,
Springer Series on Polymer and Composite Materials,
DOI 10.1007/978-3-319-23663-6_1

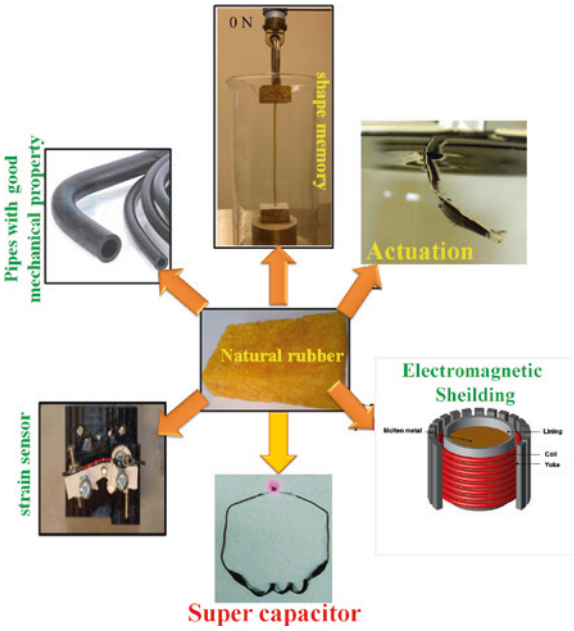

1 Introduction

Natural rubber (NR) is one of the most important biosynthesized polymers displaying excellent chemical and physical properties. Among other rubbers, it was the first industrially exploited [1, 2]. This elastomer has tremendous applications in various areas [3–5]. The source of this polymer is *Hevea Brasiliensis* tree and is present in the form of a chemical-free biomacromolecule, natural rubber latex (NRL). NRL is a stable colloidal dispersion of cis-1,4-polyisoprene (PI) of high molecular mass in aqueous medium and can be stabilized with ammonia. The highly stereo-regular microstructure of NR provides unique mechanical properties

S. Thomas
School of Chemical Sciences, Mahatma Gandhi University, Kottayam 686560, Kerala, India

S. Thomas
Center for Nanoscience and Nanotechnology, Mahatma Gandhi University,
Priyadarshini Hills P.O, Kottayam 686 560, Kerala, India

M.A.-A. AlMa'adeed
Materials Science and Technology Program, Qatar University, P.O. Box 2713, Doha, Qatar

(high elasticity) and crystallizing nature [6–10] to it. NR molecules consist mainly of cis-PI units without any trans configuration, in contrast to the synthetic polyisoprenes [11]. The very flexible backbone leads to very low glass transition temperature (T_g) of about −64 to −70 °C. Raw NRL finds wide applications in manufacturing medical products such as gloves, condoms, and safety bags due to its excellent elasticity, flexibility, antivirus permeation, good formability, and biodegradability [12–14]. However, NRL products that have short shelf lives and life cycles [15, 16] especially for medical gloves and condoms, low tensile strength, poor tear resistance and low resistance to burning [17, 18] are observed. Even though these drawbacks sound no problem for the medical products, industrially important materials such as tyres require superior performance. Due to this, several attempts to incorporate graphene, carbon nanotubes (CNTs), carbon black (CB) [19], ultrafine calcium carbonate [20], modified montmorillonite (MMT) [21], silica [22], and starch [23] fillers in dry NR or NRL [24] have been reported [25, 26].

Based on the dimensions of filler materials, it can be macrosized, microsized, and nanosized. For nanosized fillers, still the classification depends on the structure or dimension. More specifically, layered clay minerals and graphene sheets come under one-dimensional fillers, nanotubes and nanofibers are two-dimensional, and spherical particles are three-dimensional [25, 27–36] based on the number of dimensions in nanorange. Nanocomposites will be formed if one of the reinforcing filler phases has its dimension in the nanometer range. For nanofillers, maximum improvement in combined characteristics is generally observed at low loading levels, without significantly increasing the density of the compound or reducing light transmission. For instance, when the microsized fillers having lower surface area at 10–30 wt% loading impart good properties to the NR matrix, the nanofillers at 2–3 wt% loading can give superior properties due to its high surface area [37, 38]. The high reinforcing efficiency of nanofilled rubber composites, even at low loading of filler, can also be attributed to the nanoscale dispersion and the very high aspect ratio (length-to-thickness ratio) of the filler [39–43]. So the use of nanofillers in regulating the performances of NR products by alleviating the aforementioned disadvantages of NR is very fascinating and has great interest. The effect of two-dimensional nanoclay with high aspect ratios on NR microstructure when stretched was studied by Carretero et al. [44, 45] and by Huang and coworkers [46, 47]. Also, the reinforcement mechanism of NR composites with nanoalumina [48], carbon nanofibers [49], cellulose nanofibers [3, 50], and kaolin and silica [51] was studied extensively. Renewable and biodegradable biomaterials such as cellulose [52–54] consist of crystalline nanofibers of 10–40 nm diameter and 1.5 g/cm^3 density with a length of few micrometers. Such nanofibers possess high value of tensile strength (10 GPa) and Young's modulus (134 GPa) [55].

Out of the several techniques of filler reinforcement of NR, melt intercalation [37, 56], latex compounding [38], and solution-mixing methods [57] are the most common. In the nanocomposites, the dispersed nanofillers make some structural reinforcement which is responsible for the enhanced chemical and physical properties. Nair et al. [58–60] have found a three-dimensional filler network within

the NR matrix responsible for the high solvent resistance and mechanical properties, when nano crab chitin whiskers were used as reinforcement. However, direct methods of reinforcement have certain limitations to reinforce NR with fillers of higher specific surface such as spherical inorganic nanoparticles. This is probably because of the necessity to solve strong self-aggregation of nanoparticles prior to composite manufacture [61–63]. In order to achieve significant nanodispersion, self-assembly process is reported for NR/silica (SiO_2) nanocomposite preparation which could achieve better thermal properties [64].

Discovery of conducting fillers such as CNTs has opened up another way to fabricate conducting rubbers. CNTs can be regarded as rolled-up graphene sheets with essentially sp^2 hybridized carbon units in the form of cylinders with nanodiameters [65–70]. The extraordinary mechanical, thermal, and electrical properties of these nanomaterials make them potentially applicable in material science, optics, and electronics. Though CNTs prove to be ideal candidates to enhance NR properties [71], simple mixing methods were reported to be insufficient for great improvement. The general issues such as homogeneous CNT dispersion, orientations and aspect ratio, polymer morphology, CNT polymer, and CNT–CNT interfacial interactions have to be considered during composite fabrication [72]. Among the nanofillers, graphene layers also have remarkable importance in suturing the rubber properties, especially because these fillers are easier and cheaper to make compared to CNTs. The influence of graphene on the microwave properties of elastomeric composites is highly noteworthy [73–76]. In addition to CNTs and graphitic fillers, metal-coated fibers such as aluminum- or nickel-coated carbon or glass fiber and nickel-coated mica, polyaniline, short carbon fiber, and conductive CB impart conductivity to NR composites. The major electronic applications of such composites include various touch control switches, and strain and pressure sensors for applications such as robot hands or artificial limbs. Gaskets made from electrically conductive rubber composites can prevent electromagnetic induction (EMI) radiation leakage. Moreover, these materials are considered for use in different microelectronic devices and microwave applications, such as absorbing materials.

However, the above-mentioned problems associated with CNTs are often observed for all nanofillers. In order to fabricate high-performance composite products, the compatibility between the filler and the hydrophobic polymer matrix is really necessary and can be accomplished by physical or chemical modifications of the nanoparticle surfaces [10, 43, 77–83]. Using various techniques, a lot of technologically important materials have been fabricated out of NR-based composites. The objective of this critical review is to explore all electronic applications of NR composites (both micro and nano) and to highlight the high performance of nanocomposites.

2 NR-Based Composites

2.1 Synthesis Methods

The primary difficulty associated with the filler particles is to achieve a uniform dispersion in the matrix polymer, and due to this reason, processing remains a key challenge in fully utilizing the advantages of filler reinforcement. Nonuniform dispersion results in the formation of filler aggregates which can degrade the mechanical as well as physical performances of the composites through defect sites. Particle dispersions also depend on the viscosity of the medium, diffusion of particles, and particle–particle and particle–matrix interactions [84]. Better dispersion and superior properties can be achieved if the interparticle distance is comparable to the radius of gyration of the polymer. In the composite, the entire polymer matrix can be a part of an interphase and this influences processing as well. Anyway, common processing methods for polymer composites including solution processing [57], melt processing [56, 85], and reaction processing [84] are applicable for NR composites also. Latex compounding [38] method is employed especially for fabricating latex-based composites.

2.1.1 Solution Processing

Fillers (especially nano) are generally dispersed in a suitable solvent and then mixed with polymer solution by shear mixing, magnetic stirring, or sonication [86] in this technique. Sonication can be of bath (mild sonication) or probe (high-power sonication). Finally after mixing, the composite can be obtained by vaporizing the solvent. Figure 1 shows the flowchart for the solution processing. This method is considered as an effective way to prepare composite films with homogeneously distributed nanofillers [87]. However, since this method depends mostly on the efficient filler dispersion in the used solvent, the selection of solvent is rather significant. Often functionalization methods are employed in order to avoid reaggregation of fillers, and solvent selection is done on the basis of these functional groups and solubility of the polymer. Sometimes the latex can be directly used for solution mixing. This was done by diluting the NRL and adjusting the pH. The fillers in this case would be made in such a way that with addition, NRL composite will precipitate [88].

2.1.2 Melt Processing

The main principle behind this method is softening of rubber when heated. During this process, rubber transforms into viscous liquid, and at this state, additives can be well mixed into the melt by rheological shear mixing [87]. In addition to

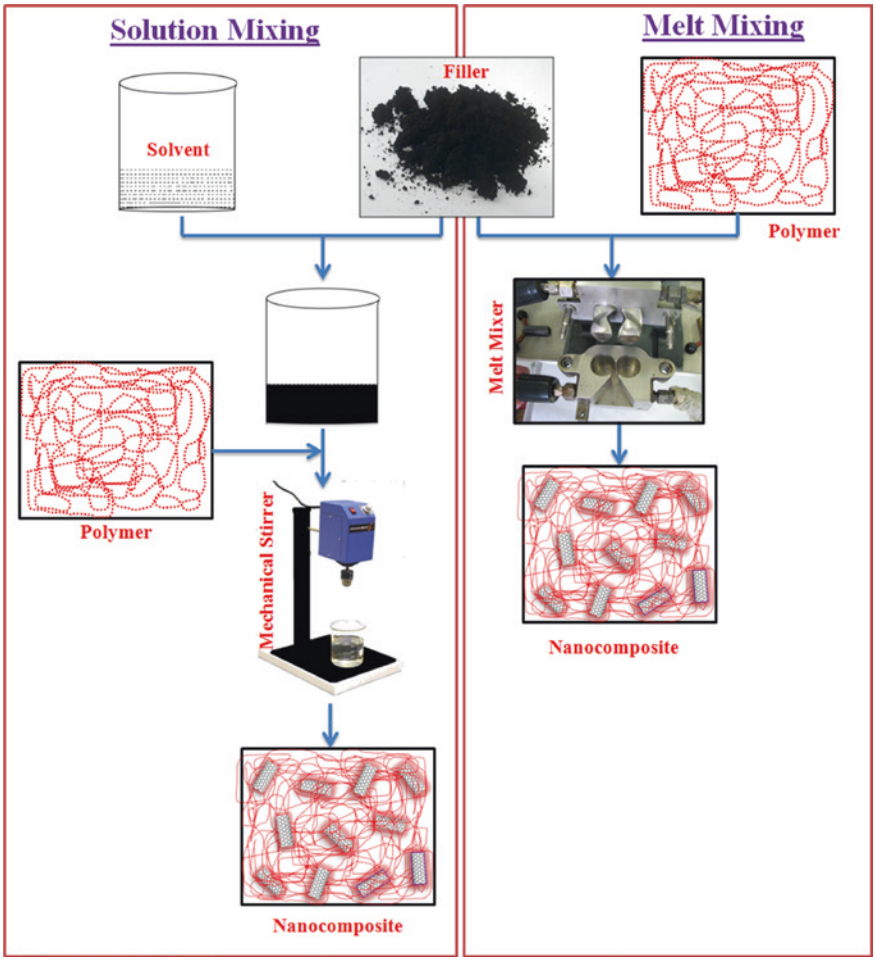

Fig. 1 Flowchart presenting the different steps of the solution and melt mixing processing of a polymer composite

the common melt mixers, large extruders are also used for bulk sample mixing. The process of melt mixing is also included in the flowchart (Fig. 1). Starch/NR/clay nanocomposites were prepared via melt extrusion technique in a high-speed mixer [10, 89]. Open two-roll mill mixing was also practiced at room temperature. The vulcanization ingredients, plasticizers if any, and fillers were added to the elastomer during mixing. NR composite containing clay or organoclay, and octadecylamine in the absence of clay was synthesized, and its effect on the cross-linking degree of NR is investigated [90]. In short, the melt mixing possesses the advantages of speed and simplicity, and compatibility with standard industrial techniques [91, 92].

2.1.3 Latex-Stage Compounding

Fillers along with curing agents such as sulfur in the presence of ZnO, stearic acid, TMTD, MBTS, etc. are compounded with NRL. At first, the curing agents are mixed (or compounded) with NRL followed by filler dispersion. This process improves cross-linking between the polymer chains in the nanocomposites, and thus, better properties can be achieved [38]. Even though in situ polymerization method is another efficient method to significantly improve the dispersion of fillers in polymers and to achieve stable filler–polymer interaction, for NR little reports exist on this. This is because of the availability of NR in its polymer form and the difficulty in controlling the polymerization of isoprene into cis-polyisoprene. Various methods to synthesize NR/CNT composites are discussed by Ponnamma et al. [42] in their review.

2.2 NR Composite Applications

2.2.1 Electromagnetic Interference Shielding

Metals are generally used to shield unwanted electromagnetic (EM) radiations; however, their heavy weight, high cost, and corrosive nature demand the need of cheaper polymeric materials. Though polymers are insulating, conducting nanoparticles produce their nanocomposites possessing good shielding effectiveness (SE). There is an increase in demand for the EMI shielding particularly at low-frequency range (30 kHz–1.5 GHz) due to a significant increase in the use of portable wireless devices such as cell phones and radios which interfere with increased sensitiveness [93]. Due to the structural and electrical advantages of nanocarbon materials, these are largely used to fabricate EMI shielding. Before going to the experimental details of the shielding materials, the theory behind EMI shielding is discussed here.

Figure 2 shows the experimental setup used by Zhang et al. to calculate the EMI SE of CNT-filled shape memory polymer. This setup is the same for NR samples as well. In general, all devices contain a network analyzer, transmitting horn antenna, and a receiving waveguide probe as shown in the figure. According to the

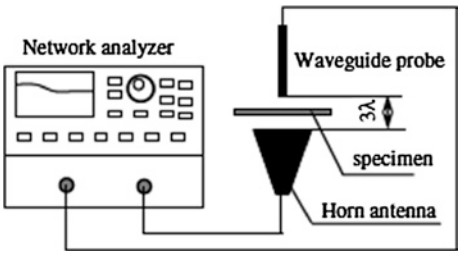

Fig. 2 The schematic of an EMI shielding effectiveness measurement system [94]. Copyright 2007. Reprinted with permission from Elsevier

frequency to be shielded, horn antenna and waveguide probe are changed. Here, the distance between the mutually perpendicular waveguide probe and the horn antenna is maintained as three times the wavelength for a given measurement frequency. The output from the network analyzer is put into the horn antenna, and the energy received after transmitting through the sample is measured by the waveguide probe. EMI SE is defined as the difference of the transmitted energy between the nanocomposite sample and a reference material. If the distance between the shield material and the source of radiation is higher than $\lambda/2\pi$, it is said to be in far field, and if the distance is less than $\lambda/2\pi$, it is in the near field [94].

The SE evaluates the reduction of EMI at a specific frequency (f) as illustrated by Eq. 1.

$$\mathrm{SE} = 10 \log \frac{P_0}{P_t} = 20 \log \frac{E_0}{E_t} = 20 \log \frac{H_0}{H_t} \tag{1}$$

where P_0, E_0, and H_0 are the energy and electric and magnetic field intensities incident on the shield and P_t, E_t, and H_t are the counterparts transmitted through the shield.

During EMI shielding, reflection, absorption, and re-reflection of the radiation can occur. These reflections as well as absorption loss depend on the electrical conductivity (σ) and magnetic permeability (μ), and such multiple reflection loss can be minimized when the distance between the reflecting surfaces or interfaces is larger than the skin depth (δ).

$$\delta = \frac{1}{\sqrt{\pi f \mu \sigma}} \tag{2}$$

SE can also be explained as the sum of reflection loss and absorption loss as shown in Eq. 3

$$\mathrm{SE} = 20 \log \frac{Z_0 \delta \sigma}{2\sqrt{2}} + 8.68 \frac{t}{\delta} \tag{3}$$

where t is the thickness of the material and $Z_0 = 120\ \pi$. If $t/\delta \leq 1.3$, the equation reduces to

$$\mathrm{SE} = 20 \log \left(1 + \frac{Z_0 t \sigma}{2}\right) \tag{4}$$

Thus, in short, the SE depends on the frequency of the radiation, thickness of the material, and resistivity. The EMI characteristics of nanocarbon particles and barium hexaferrite (BF)-filled NR are examined by Yakuphanoglu et al. The result observed by them is given in Fig. 3. The SE of the composites is frequency dependent, especially at higher-frequency range, and it increases with the increasing frequency (Fig. 3a). Variation of skin depth was in accordance with the dielectric constant of the composite (Fig. 3b). The SE also increases with filler loading (Fig. 3c) as well (0–20 wt%). As the filler loading increases and the volume resistivity decreases, the SE of the NR/BF nanocomposites increases rapidly [95].

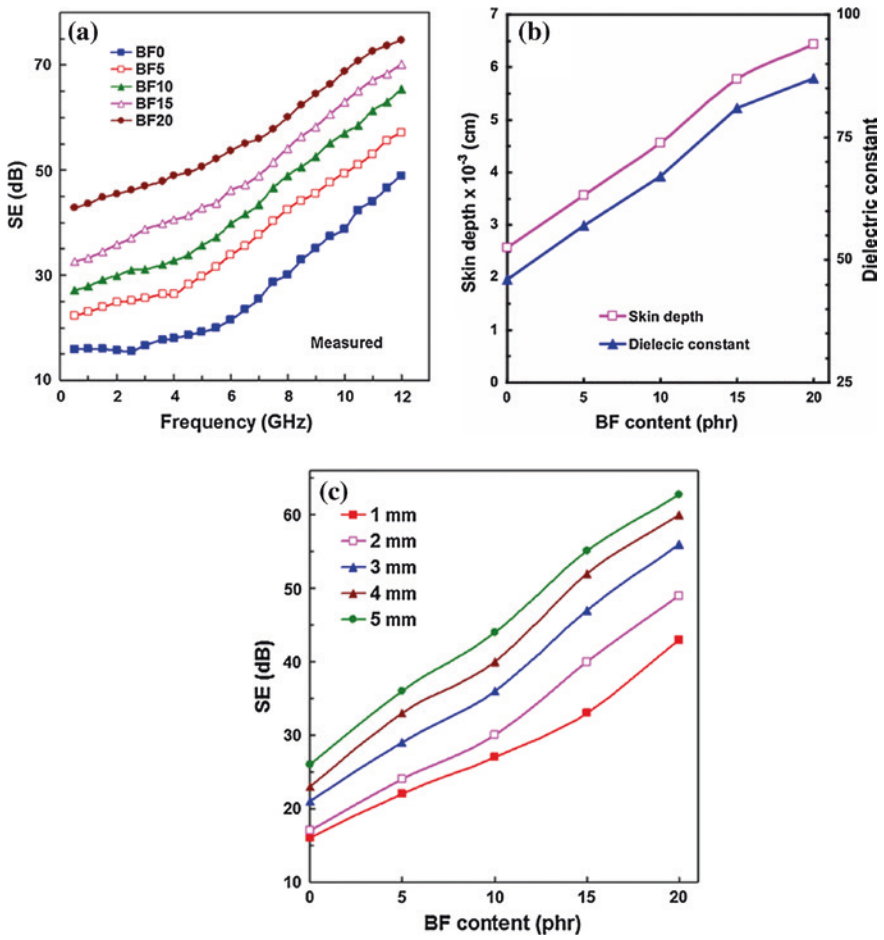

Fig. 3 **a** Shielding effectiveness as a function of frequency, **b** variation of skin depth and dielectric constant with BF content, and **c** SE with thickness of NR/BF nanocomposites [95]. Copyright 2014. Reprinted with permission from Springer

Since the EMI shielding studies are mainly based on the shielding studies of microwave radiations, this is deeply discussed in the following Sect. (2.2.2).

2.2.2 Microwave Absorption

Very recently, a large number of studies have come out on the microwave absorbing ability of NR nanocomposites. Microwave absorbing rubber composites of NR and epoxidized natural rubber (ENR), filled with conductive CB and aluminum powder, were prepared, and their shielding effectiveness was studied as shown in

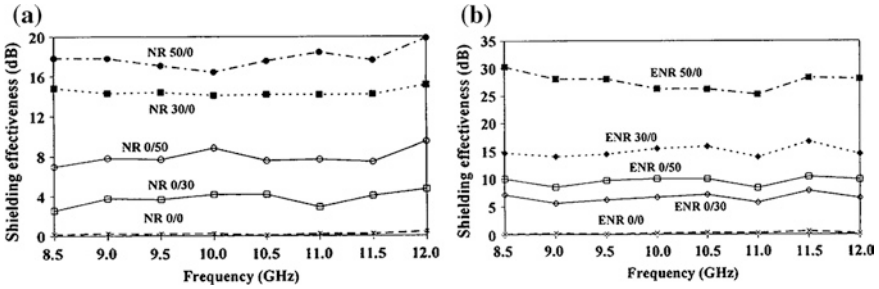

Fig. 4 Effect of single filler on SE: **a** NR composites; **b** ENR composites. The former number represents CB content, and the latter number represents aluminum powder content [98]. Copyright 2012. Reprinted with permission from Scientific Research Open Access

Fig. 4 [96]. For this, X-band microwave in the frequency range of 8–12 GHz is used. It is found that increase of filler loading-enhanced SE of the rubber composites and also the conductive CB was more effective in shielding than aluminum powder. Binary filler-filled rubber composites showed higher SE than that of single filler-filled rubber composites. SE of each sample was in the same range under the entire frequencies (8.5–12 GHz), and the effect of fillers on SE of two rubber systems was similar. Unfilled rubbers showed very low SE, <1 dB. SE of the rubber increased from <1 dB to 18–28 dB after adding 50 phr of CB or to 30–40 dB after adding 50 phr of CB and 50 phr of aluminum powder. The maximum SE of rubber composites containing 50 phr of aluminum powder (0/50 samples) was 10 dB. The SE and the mechanical properties were in the order of ENR > NR, and both these properties were correlated with electrical conductivity as well. Although the conductivity was higher, aluminum powder was less effective than conductive CB because of the lower volume fraction and larger grain size. The EMI SE of CB-filled rubber composites (50/0 samples) observed here (18–28 dB) was higher than that of other rubber composites containing 50–60 phr of the same filler CB, i.e., nitrile rubber (12 dB), ethylene vinyl acetate (EVA) (18 dB), ethylene propylene diene terpolymer (EPDM) (8–10 dB), and EVA/EPDM blend (22.5 dB).

The factors affecting the EMI SE include conductivity or polarity of rubbers and conductive fillers, filler content, particle size/shape, filler dispersion and distribution, specimen size and shape, and testing method [97]. Magnetic and microwave absorbing properties of thermoplastic natural rubber (TPNR)-filled 4–12 wt% magnetite (Fe_3O_4) nanocomposites prepared by melt blending were investigated. TPNR matrix was prepared from polypropylene (PP), NR, and liquid natural rubber (LNR) in the ratio of 70:20:10 with the LNR as the compatibilizer. The TPNR–Fe_3O_4 composites containing nanocubic spinel-structured Fe_3O_4 with 20–50 nm size showed good microwave absorption property. The absorption or minimum reflection loss (RL) continuously increases, and the dip shifts to a lower-frequency region with the increase in both filler content in nanocomposites

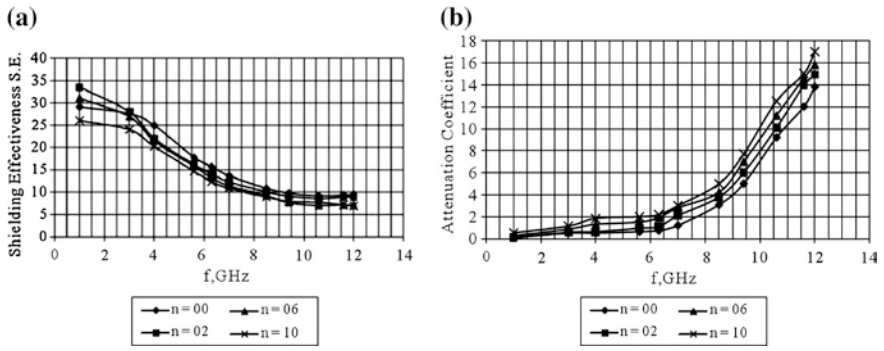

Fig. 5 Frequency dependence of **a** SE and **b** attenuation coefficient α of electromagnetic waves at various filler concentrations (n-phr of graphene) [98]. Copyright 2012. Reprinted with permission from Scientific Research Open Access

and the sample thickness. The RL is 25.51 dB at 12.65 GHz, and the absorbing bandwidth in which the RL is less than 10 dB is 2.7 GHz when the filler content is 12 wt% at 9 mm sample thickness [97]. At low frequencies, the dielectric loss in the samples is influenced by direct current conductivity, while at higher frequencies, the loss is due to alternating current conductivity. The microwave absorption properties analyzed by using peculiar absorber method reveal the existence of two matching conditions of minimum reflection due to the geometrical cancellation of the incidence and reflected waves at the surface of the absorber at low and high frequencies for the same thickness of the samples. The increment of filler content in the nanocomposites can shift the maximum attenuation to a lower frequency, increase maximum absorbing effect, and also enlarge the absorbing bandwidth. The minimum RL was found increasing and moving toward the lower-frequency region with increase in sample thickness. In short, the microwave absorbing properties of nanocomposites were determined by the thickness and the composition of filler, which can vary the dip frequency, microwave absorbing properties, and the absorbing capacity and width of the nanocomposites.

Microwave (reflection coefficient, attenuation coefficient, SE) properties of NR/GNP nanocomposites revealed interesting dependence of these parameters on frequency and filler amount (Fig. 5). The reflection coefficient increased with filler amount and frequency, whereas the attenuation coefficient was independent of frequency and filler amount in the 1–6 GHz range and increased slightly from 6 to 9 GHz and drastically in the 9–12 GHz range. The dependence was almost linear, and both the frequency and filler amount influence the SE values (10–34 dB range) as well (Fig. 5a). Since the attenuation was not great enough to compensate the increasing reflectance, the SE decreased gradually with the increasing frequency, especially up to 7 GHz. However, as a whole, the effect was more pronounced at 6–12 GHz frequency range and at 6 phr of GNP [98].

The lowering in the attenuation coefficient values (Fig. 5b) of composites is attributed to the presence of a foaming agent which makes the composite structure

porous. As a whole, the attenuation coefficient slightly increases with the increasing frequency and filler amount. The increase is particularly in the 6–12 GHz region. In the 1–6 GHz region, the effect of frequency and filler amount on the attenuation coefficient is less pronounced. This effect was in accordance with the variation observed in the complex dielectric permittivity [98].

2.2.3 Sensing Properties

Sensors based on NR composites are widely reported [68]. The sensors come under different categories such as strain sensor to detect large strains, pressure sensors to detect pressure variations, and solvent and vapor sensors to detect organic solvents and volatile components. On NR substrate, thin layer of the conducting polymer, polypyrrole (PPy), is coated by vapor-phase polymerization technique in vacuum [99] using the oxidant $FeCl_3$. This material is successfully used as a strain sensor to detect large mechanical strains, the sensing performance of which can be regulated by various parameters. Prestraining the rubber substrate prior to deposition, high concentration of $FeCl_3$, and formation of monomer vapor from diluted pyrrole monomer resulted in maximum stability, consistency, and best sensing performance of the composite. Oxygen plasma exposure produced the highest reduction in water contact angle on the rubber's surface to improve the hydrophilicity without sacrificing the rubber's elasticity and flexibility. The developed strain sensor was successfully implemented on an air muscle in conjunction with a PID controller where the extension/contraction of the muscle can be accurately controlled. It also has a capability to measure large bending strains and hence be used as a rotary sensor. The performance of the sensor can be explained by examining at the strain distribution on the NR substrate during the bending motion at different angular positions (Fig. 6). The length of the NR substrate was broken down into four segments, and the physical change in length of each segment was measured. The disadvantage of this sensor is that it shows some hysteresis.

In order to understand the strain profile of the NR/PPy sensor, the electrical resistance versus time profile is taken as given in Fig. 7a. The upward shift of the electrical resistance over the time indicates that the absolute electrical resistance value cannot be used to represent the absolute strain. So normalized $\Delta R/R_0$ values

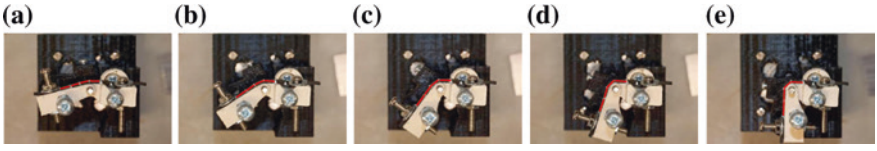

Fig. 6 The strain distribution along the length of the rubber at **a** 10°, **b** 30°, **c** 50°, **d** 70°, and **e** 90°. The different segments are represented by the *red lines* [99]. Copyright 2012. Reprinted with permission from Elsevier

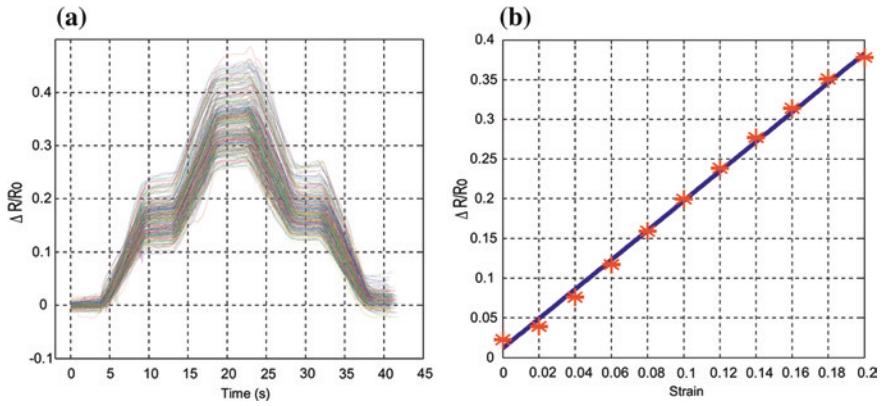

Fig. 7 **a** The change of resistance profile over 800 cycles and **b** the relationship between the strain and relative change in electrical resistance of the strain sensor from linear motion strain [99]. Copyright 2012. Reprinted with permission from Elsevier

were determined and plotted against strain (Fig. 7b). The sensitivity can be calculated by gauge factor (GF) which is defined by Eq. 5.

$$\mathrm{GF} = \left[{(R - R_0)}/{R_0}\right] \Big/ \left[\left({L - L_0}/{L_0}\right)\right] \tag{5}$$

where R is the final resistance and R_0 the initial resistance of the sample which varies its length from L_0 to L over the application of strain.

From Fig. 7b, the gauge factor for NR/PPy sensor is calculated to be approximately 1.86. The $\Delta R/R_0$ of each strain value was averaged to determine the mathematical relationship between the averaged $\Delta R/R_0$ and strain.

However, nanocomposites of NR extend stable and reversible piezoresistive strain sensing over 3000 tested cycles upon applying a small compressive strain (~16.7 %) under a relatively high frequency (0.5 Hz, 2 s/cycle). This is done by adding CNT and carbon nanofibers in NR composites pretreated with CB. The large reinforcement effect makes this composite suitable for heavy-duty pressure sensors, i.e., healthy motion monitoring of industrial machinery vibrations [100].

The strain profile of the CNT/graphite flake-sandwiched NR sensor is illustrated in Fig. 8a. The resistance increases with strain, and the CNT sensor (because of the smaller CNT size) showed higher measurable strain limit (620 %) compared with the graphite sensor (246 %). The sensitivity was calculated by GF as given in Eq. 5. The sensitivity values for the MWCNT sensors were 5.5, 10.2, 16.3, 23.1, 31.5, and 43.4 at 100, 200, 300, 400, 500, and 620 % strain, respectively, where as for the graphite sensors (Fig. 8b) the values were 23.7, 37.5, 148.1, and 346.6 at 50, 100, 200, and 246 % strain, respectively. The responses over time were checked by attaching one end of the MWCNT strain sensor to a disk, which was rotating with an angular velocity of 2 rad/s. The results obtained are given in Fig. 8c where the applied sinusoidal strain (with a period of ~3.04 s) ranged between 150 and 500 %, and the total number of cycles was more than 400 [101].

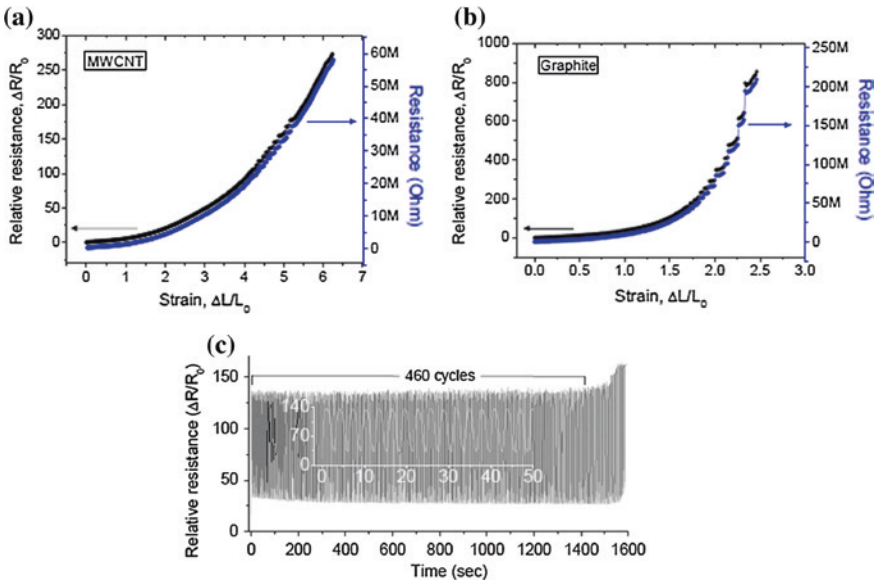

Fig. 8 Relative resistance versus strain response curves for the **a** MWCNT sensor, **b** graphite sensor, and **c** multiple cycle tests for the strain range of 150–500 % (*Inset image* the first 16 full cycles carried out over a time period of 486 s) [101]. Copyright 2014. Reprinted with permission from MDPI

The superior mechanical and electrical properties of CNTs became the basis for fabricating large number of sensors. Their nanoscale electrical properties are often related to the mechanical deformation as in the previous case [68, 102]. Macroscale strain sensor based on PI-MWCNT composites (PMCNTCs) was prepared. Better dispersion of the nanoparticles was ensured by dispersing CNTs in chloroform and thereafter mixing with the PI matrix solution. About four orders of magnitude of nonreversible change in the electric resistivity at large (40 %) stretch were observed due to the entangled structure of nanotube, thus making the PMCNTC an attractive tensile and compressive strain sensor. On the other hand, the high structure carbon nanoparticles have shown about six orders of magnitude of reversible change in the electric resistivity at large (40 %) stretch. This is due to the high porosity of carbon agglomerates which provides better adhesion to polymeric globules and mobility of nanoparticles. The maximum change at stretch for both types of composites was observed near the percolation threshold. PMCNTC can be used for small tensile strain sensing, but high structure CB–PI composite are preferable for large tensile strain sensing. The resistance of the composites was examined with regard to the force of stretch F and the absolute mechanical deformation in the direction of the force. No variation in the electric resistance was found for the samples with 7.7 mass parts of highly structured carbon black (HSCB) and 3.63 mass parts of MWCNT even at 100 % deformation of the composite. Similarly, there was a relatively weak dependence of R on the

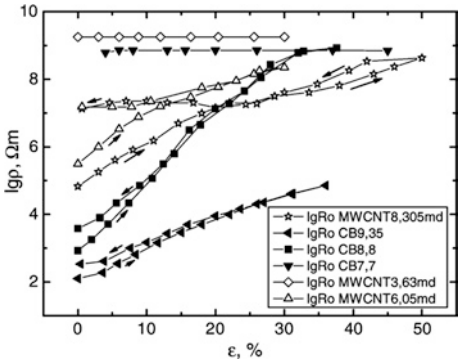

Fig. 9 The electric resistivity ρ of the PI–MWCNT composite and PI–HSCB composite versus small tensile strain ε [102]. Copyright 2007. Reprinted with permission from Elsevier

deformation at 9.35 mass parts of HSCB. Figure 9 clearly shows the variation in resistivity of different samples with respect to strain percentage.

Of all the composites examined, the best strain performance was obtained for the samples with 8.8 mass parts of HSCB and 8.3 mass parts of MWCNT, respectively, which belong to the region of percolation threshold. The resistivity of these samples changed more than six orders upon a 40 % stretch for 8.8 mass parts of HSCB composite and more than four orders for 8.3 mass parts of MWCNT composite. When the materials are released, the resistivity of HSCB composite returned to its previous value, while in the case of MWCNT composite, a relatively large hysteresis of $\rho(\varepsilon)$ was observed because of the entangled structure and high stiffness of nanotubes.

In another study, novel biocompatible NO sensor was made by spin trap (iron(II)-diethyldithiocarbamate complex, FeDETC) incorporated in a latex rubber matrix [103]. The sensor was optimized for the latex rubber matrix temperature of polymerization and FeDETC concentration inside the matrix. The NO trapped in the sensor can be detected by electron paramagnetic resonance (EPR). The EPR signals showed variation with respect to different conditions. The best sensor was made with a latex rubber matrix polymerized at 10 °C and with a FeDETC concentration of 14.8 mM. High stability of the EPR response was detected for 40 days at room temperature.

2.2.4 Dielectric Property

Neat NR is an insulator, but it becomes conductive when conducting nanoparticles are incorporated in it. In addition to the electrical conductivity, some of these composites are good dielectric materials as well. NRL composites with polyaniline (Pani) were prepared by the in situ polymerization of aniline in the presence of latex [104]. The dielectric properties of different compositions of the samples in microwave frequencies were determined (Fig. 10a).

From variation of the dielectric constant with frequency (S bands 2–4 GHz) of Pani–NR semi-interpenetrating networks, it is clear that the dielectric constant was

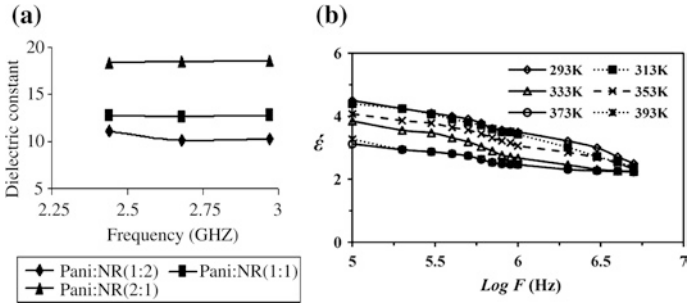

Fig. 10 **a** Variation of dielectric constant with frequency for the Pani–NR composites [104]. Copyright 2007. Reprinted with permission from John Wiley & Sons. **b** Dielectric constant for NR as a function of frequency at different temperatures [105]. Copyright 2012. Reprinted with permission from John Wiley & Sons

less affected by frequency. But the value changes from NR (i.e., 2) to Pani–NR, the maximum shown for the 2:1 composition. The absorption coefficient and penetration depth calculated for 2:1 composition were, respectively, the highest and the lowest. NR allowed the passage of electromagnetic radiation, and when the Pani content was increased, the electromagnetic radiations were restricted to penetration. The in situ technique also contributes toward high dielectric constant. The conducting NR could be used in various applications, including antistatic coatings, antistatic chappels, and anticorrosion applications.

Figure 10b shows the effect of both frequency and temperature on the dielectric constant for NR [105]. Both dielectric constant and tan δ of NR are less dependent on frequency and temperature due to the absence of polarization and ionic properties of the material. Since NR is a nonpolar molecule, its dielectric constant will be the square of the refractive index (1.59) [106, 107]; however, the experimental value obtained is higher than the theoretical one due to the presence of interfacial polarization which arises due to the presence of impurities such as the compounding ingredients. At high frequencies, the values become about 2.5 for all temperature ranges, which can be ascribed to the mobility of a polar group in the polymer chains, which is too slow to contribute to the dielectric constant at high frequencies. By following the experiment, the dielectric constant, dielectric loss, and tan δ of barium ferrite–NR composites were studied [105]. All these values decreased as the frequency increases, and at higher frequencies, the effect significantly weakens. ε' for barium ferrite was related to the preparation method, and at lower filler loading, the ferrite content strongly influences the dielectric properties. Up to 30 Phr ferrite loading, ε' sharply increases, and thereafter, the dependence of ε' on ferrite content becomes minimal as a result of ferrite particle interaction. Ferrite content also enhanced the dielectric loss and tan δ. They could observe a strong correlation between magnetic initial permeability and dielectric constant for hard magnetic material polymer composites as well.

Oil palm fibers were modified with silane, and the effect of modification on dielectric properties of NR is checked for the biocomposite. At low level of fiber loading (20 %), the dielectric properties show only a nominal change, and with fiber treatment, the loss factor increases [108]. Even though the effect of the oil palm fibers and their chemical treatment with silanes on the dielectric properties is evidenced well, other factors such as fiber orientation and quantity of chemical used were not addressed in this work. For the sisal/coir hybrid fiber-reinforced NR composite, the dielectric constant values were higher due to the polarization effect induced by fibers' incorporation. The lignocellulosic fiber addition increased the number of polar groups and decreased the volume resistivity of the composites. At 15.6 % volume, percolation threshold is reached. Upon increase in frequency, the interfacial and orientation polarization decreased and thus the dielectric constant [109].

Fiber treatment, such as acetylation, benzoylation and reaction with alkali, peroxide and permanganate were carried out to improve the adhesion between fibers and matrix. Modification also reduces the moisture absorption capacity of the fibers due to reduced interaction between polar –OH groups of lignocellulosic fibers and water molecules. For composites containing chemically treated fibers, the dielectric constant values were found to be lower for all frequencies due to the increased fiber hydrophobicity. Chemical treatment increased the volume resistivity of the composites as well. In the untreated state, the –OH groups of fibers form strong hydrogen bonds and are thus unreactive. Alkali treatment destroys the hydrogen bonding and makes them more reactive and leads to decreased orientation polarization. It also can lead to fibrillation and thus can enhance the surface area [110]. This is the reason why alkali-treated fibrous composites showed considerable decrease in dielectric constant. In composites, the fibers and NR matrix interlock each other. The addition of two-component dry bonding agent consisting of hexamethylenetetramine and resorcinol improved the interfacial adhesion between the matrix and fibers and reduced the dielectric constant. It also enhanced the electrical resistivity and dissipation factor of the composites. The added fibers and different chemical treatments for them increased the dielectric dissipation factor. A dielectric relaxation has been observed at a frequency of 5 MHz. The dielectric constant of treated fibers decreases in the order, alkali > acetylated > benzoylated > permanganate > peroxide > bonding agent [106]. The conductivity of the composites was also found to increase with increase in fiber loading as the number of conductive particles increased. Finally, the application of such low-cost composites in antistatic materials is explained. Depending on the concentration of alkali, the dielectric constant varies. Fibers treated with 4 % alkali showed the lowest value. Of the three types of silanes, fluorosilane and vinyl silane, respectively, exhibit the minimum and maximum dielectric constant. Mercerization prior to silane treatment is an effective means of attaining better property retention to composites exposed to moisture. Silane coupling agents have inherent natural attraction with both the natural fiber and resin matrix [111].

Effect of alumina particles on the properties NR revealed the ionic polarization of the microalumina particles and the induced dipole moments set up in the

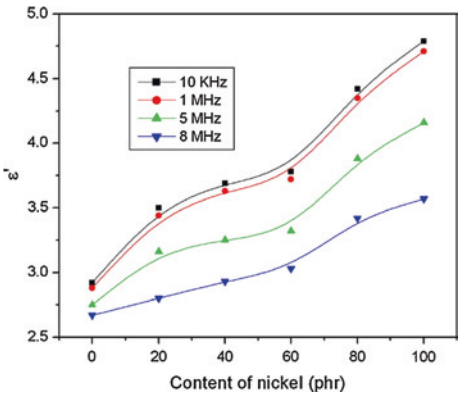

Fig. 11 Variation of permittivity with content of nickel in the composites per hundred weight ratio of rubber (phr) is plotted in the horizontal axis [119]. Copyright 2009. Reprinted with permission from Elsevier

matrix. At 0.00968 volume fraction, the composite showed the highest dielectric constant of 2.123 and the electrical conductivity of 2.683×10^{-8} $(\Omega.m)^{-1}$. The soft and flexible composites containing small amount of alumina can store additional elastic energy within the matrix under electric field and are useful in fabricating biomimetic actuators and/or artificial muscles. ε' of magnetic NR composites containing uniformly distributed nickel nanoparticles decreased with increase in frequency and increased with increase in nickel loading (Fig. 11). Metallic inclusions in any insulating material enhance the dielectric permittivity of the material as reported [112, 113]. Interfacial polarization due to the heterogeneity of the samples is attributed as the reason for the variation of dielectric permittivity with frequency as well as filler concentration [114]. The dielectric dispersion observed in the frequency range of 100–8 MHz at 40 °C shows the linear increase in permittivity with the nickel particle loading. Here, the dielectric loss in the material is small and can be useful in making capacitors. The mechanism of ε' is understood by interfacial polarization, enhancement of electrical conductivity [115], and formation of internal barrier layer capacitors [116, 117]. Interfacial polarization arises at the interface of a composite with electrical heterogeneity due to the migration of charge carriers through different phases, and charges accumulate at the interface [118]. External electric field moves these charges, and motions prevented within the medium cause polarization.

Permittivity increases with filler loading almost linearly with all frequencies and at all temperatures. Dielectric loss of blank rubber, as well as the composites, was observed to increase with temperature [119]. The decrease in permittivity with temperature is attributed to the high volume expansivity of rubber at elevated temperatures. Dielectric loss of the composites was found to increase with temperature, and a relaxation peak was only observed in blank rubber. For filled samples, the dielectric relaxation peaks appear to exist below 100 kHz. A weak interfacial polarization present in the rubber matrix can be attributed to the observance of relaxation peaks in blank rubber.

In another work, the relaxation phenomena occurring in NR and polyurethane (PU)/NR blend-based nanocomposites, reinforced by layered silicates, were

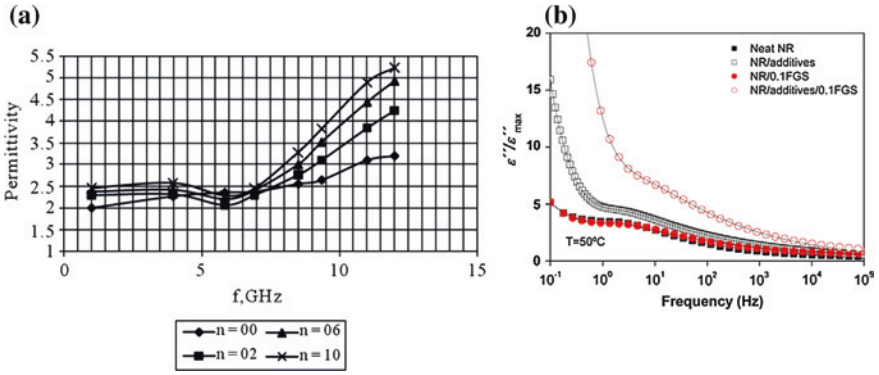

Fig. 12 Frequency dependence of **a** relative dielectric permittivity ε' at various filler content (n-phr of graphene) [98]. Copyright 2012. Reprinted with permission from Scientific Research Open Access. **b** Normalized dielectric loss ε'' of the nonvulcanized nanocomposites in the normal mode. *Solid lines* correspond to HN fittings and *dashed lines* to individual processes [123]. Copyright 2012. Reprinted with permission from Elsevier

examined during 10^{-1} to 10^{6} Hz frequency. NR is nonpolar, and its performance is only slightly affected by the presence of layered silicates. It has low dielectric permittivity and loss, and its relaxation is visible in the low T_g range. But PU exhibits four relaxation processes—ascending relaxation rate, interfacial polarization (IP), glass/rubber transition, and local motions of polar side groups and small segments of the polymer chain. Both matrix and filler influence relaxation phenomena, and IP is present in all nanocomposites being the slowest recorded process [120].

The influence of graphene nanoparticles (GNPs) [98] at 2.0–10.0 phr on the dielectric properties (dielectric permittivity, dielectric loss angle tangent) of NR nanocomposites has been investigated in the wide frequency range (1–12 GHz). The dielectric permittivity increased slightly with the increasing frequency and filler amount, especially significant in the 9–12 GHz range. The tendency was the same in the case of dielectric loss angle tangent, although the impact of the filler amount is less marked, i.e., the imaginary part of the complex relative dielectric permittivity is less sensitive to alternations of the filler amount and frequency than the real part. Figure 12a shows the frequency dependence of the real part of the complex relative dielectric permittivity. The close dielectric permittivity value for various filler concentrations up to 7 GHz is clearly seen. As explained at >7 GHz, the values show significant difference between the nonfilled and filled composites. The values obtained for the nonfilled composites are close to the ones for NR at 1000 Hz reported, which are 2.40–2.70 [121]. At higher than 9 GHz, the high dielectric permittivity comes mainly due to the composite polarity [122].

The effect of functionalized graphene sheets (FGSs) on the dielectric properties of NR nanocomposites is illustrated in Fig. 12b. The shift toward higher frequencies is observed in the presence of the additives and becomes more significant with FGS. Molecular dynamics of NR is often affected by vulcanizing additives which

can decrease the segmental motions [123]. FGSs have defects, free radicals, and other irregularities on its surface and thus cause strong rubber–filler interactions. These interfacial interactions accelerate the cross-linking reaction and increase the electrical conductivity.

Those rubber–filler interactions are also reflected by the changes in the time-scale of the global chain dynamics (normal mode) in NR/FGS nanocomposites. The figure gives the effect of FGS on NR in the normal mode. The normal mode is assigned to the chain dynamics and, consequently, is strongly dependent on the molecular weight and on the mobility of the chain-end cross-links in the naturally occurring network of the NR. The final material having multifunctional property enhancements coupled with low cost and large-scale production makes wider applications for it.

2.2.5 Thermal Conductivity

CNTs are reported to be excellent in improving the thermal conductivity of NR which is also significant in electronics. In situ measurements of thermal conductivity, heat capacity per unit volume, and T_g of pure PI and PI/single-walled carbon nanotube (SWCNT) composites cross-linked by high-pressure treatment (4 h at 513 K and 1 GPa) revealed the enhancement in thermal conductivity of both the elastomeric and liquid PI by ~120 % at 5 wt% SWCNT loading [124]. T_g of the cross-linked elastomeric state increased by 12 K and that of the liquid PI by ~7 K at the same filler concentration. CNTs enhanced broadening of T_g in the high-pressure-treated densified elastomeric states but not in the untreated samples. The increase observed for cross-linked state can be attributed to the filler-induced increase in the cross-link density. The heat capacity decreased by ~30 % in both the glassy and liquid/elastomeric states (above and below T_g) due to the large reduction in the vibrational and configurational heat capacity of PI in the presence of SWCNTs. It is also observed that the thermal conductivity (κ) of the composite linearly increased with SWCNT content. Also, the pressure-induced densification decreases the interparticle (CNT–CNT) distances without agglomeration and improves the thermal and electrical contact between the constituent materials of the composite. In the case of a semicrystalline polymer, high-pressure treatment can increase the degree of crystallinity and thus can strongly enhance the thermal conductivity of the matrix. Thus, thermal as well as electrical percolation networks in polymer CNT composites and the nature of thermal and electric transport in them are better studied by high-pressure treatments.

Variation of κ with temperature at 0.02 GPa is shown in Fig. 13a. All samples show similar amorphous behavior where κ is almost constant or slightly increasing with temperature. A small peak is also observed distinguishing two temperature ranges, which is most apparent in PI-SWCNT5. Below the peak, κ moderately increases with temperature, whereas above the peak it becomes temperature independent. More than three times larger change for PI-SWCNT5 is noted compared to PI. For pure PI, the change is less pronounced. The change occurring in κ with

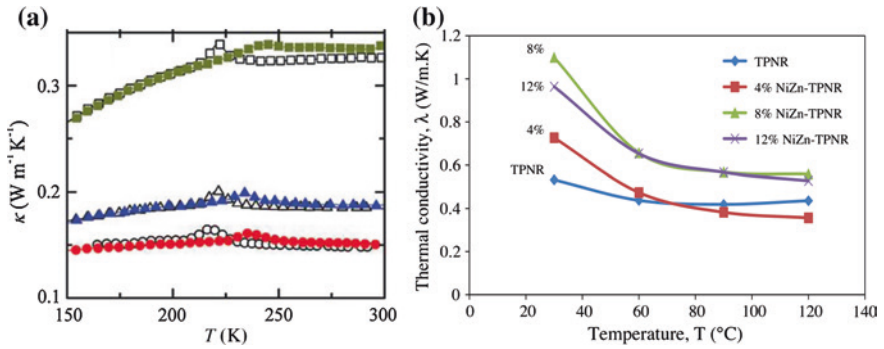

Fig. 13 **a** Simultaneously measured results for thermal conductivity [124]. Copyright 2009. Reprinted with permission from American Chemical Society. **b** Thermal conductivity dependence on temperature for TPNR and different loaded NiZn–TPNR nanocomposite samples at 30, 60, 90, and 120 °C [126]. Copyright 2013. Reprinted with permission from Elsevier

Table 1 Thermal conductivity of NR nanocomposites

Sl. No.	Type of filler and concentration (wt%)	Thermal conductivity W/(mK) (composite/neat)	References
1	RGO at 5	0219/0157 for solution treated 0188/0157 for mill mixed	[128]
2	Alumina and boron carbide at 12	09/02	[129]
3	Graphene at 2	01963/01741	[130]
4	Nanosilica at 20	0133/0097	[131]
5	Nanographene platelets at 2	2130/013	[132]

respect to temperature is attributed to the thermal expansivity increase at the T_g and the stronger decrease in density above T_g than below [125]. High-temperature and high-pressure treatment causes changes in the number of covalent bonds between the chains, density, and structural order, and affects κ values. During the treatment, both chain scission and cross-linking can occur, and the density as well as the order can decrease or increase due to decreased or increased degree of crystallinity. But here, the authors have ruled out the possibility of chain scission because of sample cross-linking. Comparison of samples of pure PI cross-linked at 1 GPa and 0.5 GPa by submerging in water–methanol mixture revealed that the samples become progressively denser with increasing pressure of the high-temperature treatment. The sulfidic and carbon–carbon cross-links further decrease the already weak tendency of cold crystallization in PI. Since PI is difficult to crystallize, the major part is inevitably amorphous and the difference is likely small. Moreover, a decreased crystallinity would also decrease κ. The increase in κ at room temperature and near atmospheric pressure is therefore attributable to the increased number of covalent bonds between the chains and increased density. The κ values for a few NR nanocomposites are given in Table 1.

Thermal conductivity dependence of NiZn ferrite nanoparticles filled TPNR magnetic nanocomposite on temperature is given in Fig. 13b. TPNR was prepared from NR, LNR and high-density polyethylene (HDPE) in 20:10:70 ratio by melt blending [126]. Tremendous enhancement of thermal conductivity with increasing filler content up to 8 % of NiZn ferrite is observed, and thereafter, κ decreased slightly with filler content. The calculated enhancement in κ for 4, 8, and 12 wt% NiZn–TPNR nanocomposite samples was about 38, 108, and 81 %. The increase of thermal conductivity with filler rates could be attributed to the nature of NiZn ferrite nanoparticles, which are assumed to have a higher number of phonons' vibrational modes as well as higher mean free path due to its crystalline structure compared to the amorphous TPNR matrix. Also, the incorporation of NiZn ferrite nanoparticles creates a percolated network facilitating the phonon conduction inside the nanocomposite and therefore enhances κ [127]. Moreover, the T_g value of the TPNR matrix increases with filler content, suggesting an enhancement in the thermal stability of the TPNR matrix. Thus, 8 wt% filler content remarks the optimum filler concentration in the formation of the percolated network, above which κ value decreases. The decreasing trend in κ value for all nanocomposite samples with temperature is due to the increase of structural defects existing in the amorphous behavior of TPNR matrix, which damp the phonons' vibrational amplitudes.

2.2.6 Shape Memory Materials

Shape memory polymers (SMPs) are smart, responsive materials having numerous potential applications in various fields and in electronics [133]. Shape memory natural rubber (SMNR) has much importance among other SMPs in exhibiting exceptional properties such as strain storage of 1000 %, cold storage, cold programmability, and mechanical and thermal triggers tunable both during and after programming. They also possess energy storage capability and mechanical properties. SMNR decreases the melting temperature of crystals up to 40 K by the application of external mechanical stress. The mechanical stress parallel to stretching direction stabilizes the crystals indicated by linear increase in the trigger temperature, whereas the stress applied in the transverse direction weakens the shape-stabilizing crystals and resulted in decrease in the trigger temperature after programming (stress-induced melting). The reinforcing effect of parallel stress on the shape-stabilizing crystals is called stress-induced stabilization. A significant amount of crystals still exist in the stretched SMNR above the trigger temperature as evident from the XRD measurements. Above 100 °C temperature, this completely disappeared. Fukahori proposed the existence of partially continuous cross-linked phase and a continuous uncross-linked phase in vulcanized NR by which the two different melting regimes of the crystals were explained [134]. The strain-induced crystallization appears mainly in the cross-linked phase followed by thermal crystallization in the uncross-linked phase. The crystals formed in the cross-linked phase should be more sensitive to parallel stress than the crystals formed in the uncross-linked phase. This should then result in the two melting regimes.

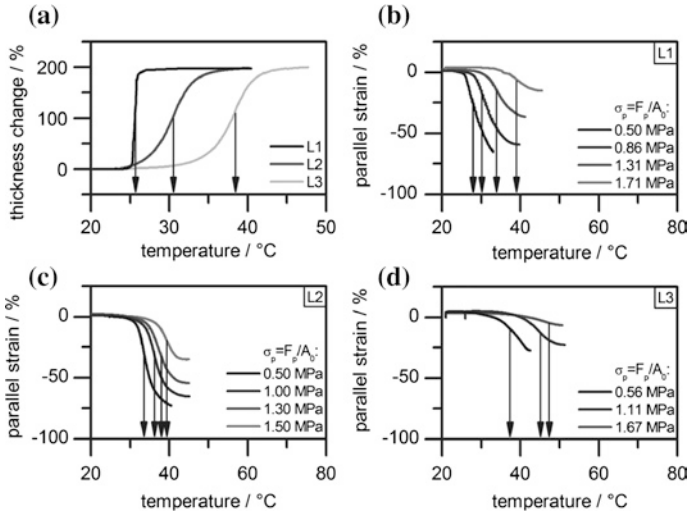

Fig. 14 **a** Determination of unstressed trigger temperatures of samples L 1–3 using TMA measurements. *Arrows* indicate different trigger temperatures (*T* trig, L1 258 °C; L2 305 °C; L3 384 °C, in all cases, the perpendicular strain increase was measured). Determination of trigger temperatures of **b** L1, **c** L2, and **d** L3 in dependence on different applied parallel stresses (in all cases, the parallel strain decrease was measured) [135]. Copyright 2013. Reprinted with permission from John Wiley & Sons

The shape memory property of two series of samples, one based on vulcanized NRL (degree of cross-linking: 0.2 %, abbreviated by L) and the other prepared by vulcanizing compacted rubber (degree of cross-linking: 0.1 %, abbreviated by NR), was analyzed at different stretching temperatures. Figure 14 shows the resulting trigger temperatures obtained from TMA measurements, which show the perpendicular strain increase during recovery for L 1–3. The average trigger temperatures (*T* trig) obtained for the samples L1, L2, and L3, respectively, were 25.8, 30.5, and 38.4 °C.

Figure 14b–d, respectively, illustrates the influence of constant stress applied parallel to prior programming direction on the samples L1, L2, and L3 [135]. All plots of parallel strain against temperature show a rising trigger temperature with increasing stress. This applied stress was significantly smaller than the stored stress, and as a result, the sample retracts to some extent upon increasing the temperature. This retraction continues until either the samples reach the limit of the apparatus or the samples rupture. The retraction process of L1 and L2 under different loads is triggered much more discrete than that of L3, which can be due to the stress-free trigger temperature ranges of the unstressed samples. The vulcanized samples NR 1–3 also follow similar results. The trigger temperature strongly depends on the stress of the surrounding amorphous phase on the strain-stabilizing crystals [136], and the parallel stress causes a stabilizing effect on the polymer crystals, resulting in an increase of the trigger temperature.

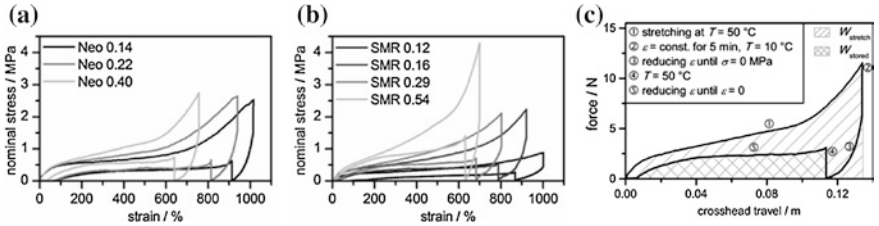

Fig. 15 Exemplary plots of nominal stress versus strain during a shape memory cycle of **a** latex-based and **b** SMR-based samples, plot of force versus crosshead travel of sample Neo 040 (dimensions: 178 mm × 382 mm × 11 mm) during a shape memory cycle [137]. Copyright 2013. Reprinted with permission from John Wiley & Sons

Figure 15a, b shows the variation of nominal stress with strain during the shape memory cycle of latex-based (Neo) and SMR-based samples [137]. The values of stored energy were obtained in a range from 1.34 to 4.88 J g^{-1} with efficiencies (ratio of stored to stretching energy) between 26.22 and 48.32 %. It is also found that the stored energies and efficiencies increase with increasing degree of cross-linking for both SMNR sources. The stored energy also depends on applied strain during programming.

The SMNR showed fixity ratios of up to 94 % and recovery ratios of up to 100 % combined with high stored strains in a range of 540–1180 % after 10 thermomechanical cycles. Energies of up to 4.88 Jg^{-1} could be stored with up to 53.30 % efficiency. This material also has excellent Young's modulus (two orders of magnitude upon triggering or programming). All these properties are observed in the case of latex-based samples as well (Fig. 15b); however, the masticated samples show superior shape memory and energy storage properties. The complete shape memory cycle of the latex-based sample Neo 0.40 is given in Fig. 15c for detailed information. The integral of the programming path 1 corresponds to the energy *W* stretch needed for stretching the rubber at 50 °C to a strain of 750 %. The elastically stored energy *W* during shape recovery at 50 °C is also equal to integral of the recovery path 5 [138].

The shape memory of NR in the presence of solvent vapors is illustrated in Fig. 16. For this, SMNR is kept in contact with toluene vapors and thus immediately triggered, resulting in complete shape recovery [139]. The programming steps showing the stretching (1) and fixation steps (2) are clear from the stress–strain plots of SMNR in Fig. 16a. Triggering the sample under unconstrained conditions resulted in strain answer (3), whereas triggering under constrained conditions resulted in stress answer (4). The solvent caused complete recovery, and so the qualitative and quantitative information on the trigger capability of the vapors is lost. The same effect was also observed in the case of other solvents such as chloroform, n-heptane, and tetrahydrofuran (THF). By mounting the programmed SMNR between a fixed clamp at the bottom and a spring scale, pulling force is determined as shown in Fig. 16b.

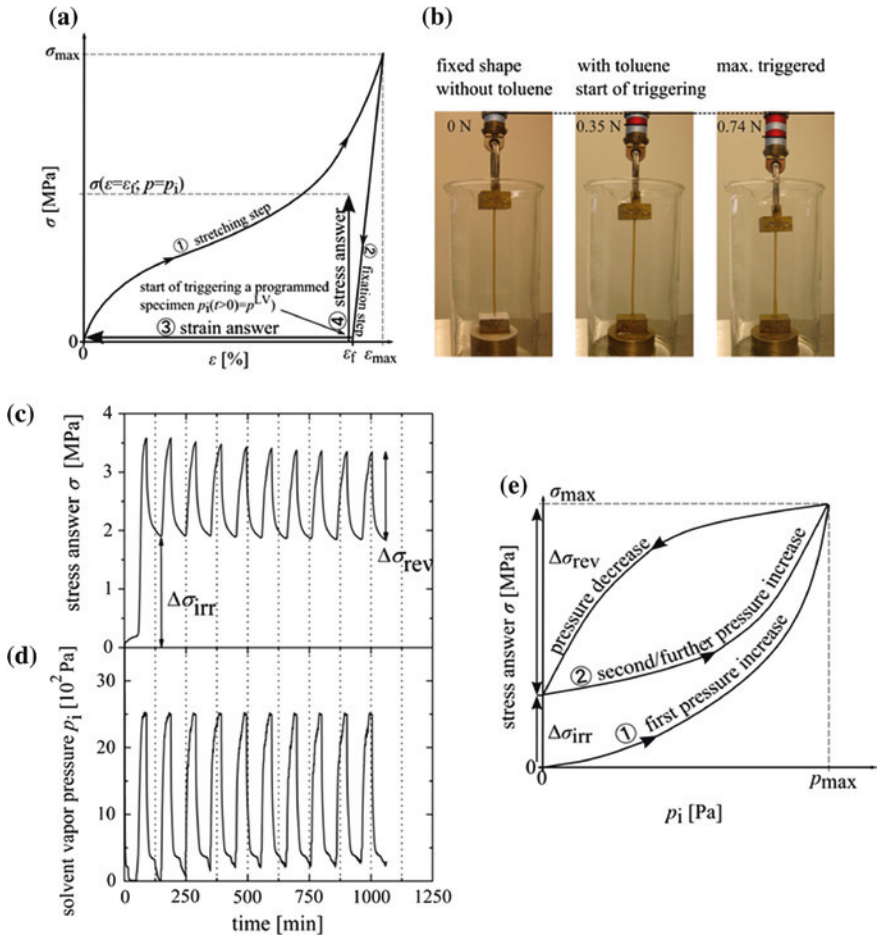

Fig. 16 **a** Stress−strain plots of the programming process of SMNR, **b** photographs illustrating the stress built up by exposure to toluene vapor temporal progress of **a** stress answer σ of constrained SMNR with **b** changing vapor pressure pi plotted, and **c** schematic illustration of the irreversible and reversible stress answers caused by the solvent vapor pressure during the first ($\Delta\sigma$irr) and all following cycles ($\Delta\sigma$rev) [139]. Copyright 2013. Reprinted with permission from American Chemical Society

In order to investigate the effect of solvent on triggering, the constrained SMNR sample was subjected to a force of about 1.7 N within 15 min, and thereafter, the unclamped sample was brought to atmospheric pressure following vapor evacuation. SMNR was not fully triggered as it did not recover its original shape, but stabilized 800 % strain. Cyclic experiment in which the stress is continuously measured by adding and removing toluene vapor pressure was further performed at constant time intervals to confirm partial triggering or triggering and reprogramming after solvent removal. As shown in Fig. 16c, the sample stress becomes

3.6 MPa upon increasing the toluene vapor pressure to 2500 Pa in the first cycle. When the vapor was evacuated below 300 Pa after 15 min, the sample stress decreased to 1.8 MPa. This two-way stress response is due to reprogramming of the SMNR sample. The results were reproducible. By comparing Fig. 16c and d, the direct dependence of stress answer on the vapor pressure increase is derived. The stress answer did not return to its initial value even after 24-h evacuation at which the stress was 1.7 MPa. Thus, the solvent-sensitive stress answer of SMNR on toluene vapor is composed of an irreversible stress answer $\Delta\sigma_{irr}$ that remains after the first cycle and a reversible stress answer $\Delta\sigma_{rev}$, as represented in Fig. 16e [140].

2.2.7 Actuators

Electroactive polymers (EAPs) convert electrical energy into mechanical energy and widely applied in actuators, sensors, motors, pumps, etc. [141]. Such dielectric and electrostrictive materials possess advantages of rapid response rates depending upon ionic diffusion, dipole moment, electrostatic forces, low operating voltage, high force generation capabilities, and high energy density per cycle, and thus, they are useful in fabricating catheters, automotive door locks, and artificial muscles for robotic and prosthetic devices and in bioengineering. Typically, the uses of actuators include adaptive optic applications to move an optical element, to connect thermal or electric pathways, and to provide agonist and antagonist controls in a linear motion, etc.

As NR composites are flexible and easily fabricable, they are also EAP. The application of an external electric stimulus to EAP induces dipole–dipole moments in molecules and thus induces electrostatic interactions between them. Higher force is required to deform such materials, which indicates that the mechanical properties of the material have been altered [141]. Niamlang et al. synthesized poly(p-phenylene vinylene) (PPV)/NR blend (10 %w/w PPV) in the presence of a cross-linker. The addition of a conducting polymer to the elastomer enhances the dipole moment of the conductive polymer and thus the interference of the dipole–dipole interactions between the cross-linking points. When external electric field strength is applied, the NR gel deflects toward anode, the functional group and strand are polarized, and ionic interaction between generated dipole moment and electrode is occurred. If the strength of the applied field is higher, stronger interaction occurs between dipole moment and electrode and causes higher degree of bending [141].

Blending NR with polythiophenes is also practiced by Puvanatvattana et al. by which they analyzed the electrorheological response of the samples to make it applicable in actuators. Electric field strength of 0–2 kV/mm was applied, and the corresponding storage and loss modulus values were noted. For PI of cross-linking ratios 2, 3, 5, and 7, the storage modulus sensitivity increased with applied field strength and attained maximum values of 10, 60, 25, and 30 %, respectively, at 2 kV/mm. For the PI/polythiophene blend, containing 5, 10, 20, and 30 vol.%, the moduli were higher than those of cross-linked PI. The storage modulus sensitivity

of such blends also increased with field strength and reached maximum values of 50, 35, 110, and 45 %, respectively, at 2 kV/mim [142].

Orthorhombic and noncentrosymmetric perovskite lead zirconate ($PbZrO_3$) capable of spontaneous polarization was synthesized at a temperature below the Curie temperature and dispersed in NR. At a volume fraction of 0.007306, the electrical conductivity of the composite increased dramatically by two orders of magnitude at 500 kHz electrical frequency. The obtained composite sample showed variations in storage modulus with applied electrical field. When the field strength was 1 kV/mm, the temporal characteristic of the neat NR increased from 9.4 kPa to a steady-state value of 9.6 kPa, whereas for the composite, the increase was abrupt (from 9.4 to 12.6 kPa). This value decreased, but not went to the original value when the field was turned off. This behavior indicates that there are some irreversible interactions, possibly due to the dipole bonding between small lead zirconate particles at this volume concentration and some residual dipole moments remaining [143].

Based on the deflection responses of a standard Thai rubber (STR) composite of Al_2O_3 cross-linked with dicumyl peroxide, Tangboriboon et al. proposed a three-stage mechanism for the electromechanical cycle of the actuator. This is shown in Fig. 17a where both electrodes have the same concentration of dopant (Al^{3+}) when the cantilever is undistorted, and the electrochemical transfer of the Al^{3+} between electrodes causes bending either to the right or to the left. The STR/alumina samples were cured using sulfur as well. They have checked the effect of cross-link agents between the sulfur/accelerator and the DCP/stabilizer on the deflection response of the composites under applied electrical field strength of 0–650 V/mm at room temperature. In the presence of applied field, the freely suspended end of the dielectric elastomer actuator bends toward one of the electrodes due to the interaction between the electrode and the nonsymmetrical dipole moments set up in the matrix. The maximum bending is observed for the DCP cured sample containing 60 phr alumina at 200 V/mm in which the dipole moment generated causes a nonsymmetrical negative charge distribution and as a result it

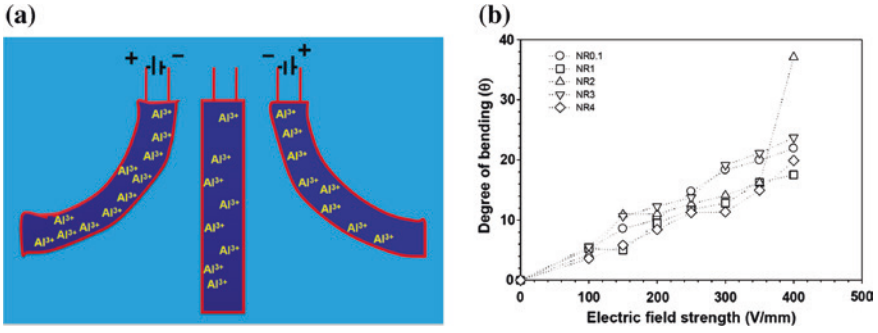

Fig. 17 **a** Three states during the electromechanical cycle of a dielectric elastomer actuator and **b** degree of bending of cross-linked natural rubber at various electric field strengths [145]. Copyright 2013. Reprinted with permission from Elsevier

bends toward anode. In addition, the alumina particles induce polarization within the composite and the dipole moments under applied electric field which results in high dielectric constant for the composites with maximum alumina content [144]. Also, the DCP curing induces better actuation effect when compared to sulfur curing [145] as per the results shown in Fig. 17b (all samples contain DCP at various percentages).

3 Conclusions

Nanotechnology offers technological advantages in various important areas, such as production, processing, storage, transportation, safety, and security. As presented in this review, the products based on NR derived from nanotechnology are applicable in electronics, aerospace science, valuable household items, value-added products, and industry. NR is an excellent polymer and obtained from nature, which has shown its own importance in the literature for long years. Nanofillers are capable of imparting superior properties such as gas permeability (impermeable tyres), electrical (conductive wires, sensors) and thermal conductivity, dielectric properties (capacitors), mechanical strength (cables, sheets, etc.), flame retardancy, shape memory, and microwave absorption properties to NR. A comprehensive as well as state-of-the-art review on NR and its composite applications has been made in this paper. Materials for piezoelectrics and low-friction lightweight devices with high durability can get at low cost. Major advantages of nanocomposites in comparison with their micro counterparts are addressed in most parts of this study. However, the fabrication of nanocomposites is often associated with filler–polymer compatibility, interfacial interaction, nanolevel dispersion, etc. Because of this, practical applications of NR composites are rather limited so far. Therefore, further developments to achieve nanofiller-reinforced composites with relatively high volume fractions and with maximum filler–polymer and filler–filler interactions are still required. For this, acquisition of fundamental knowledge and development of analytical models and experimental tools are also needed. In short, this review briefly discusses applications and summarizes the needs on fundamental research as well as the associated challenges of NR and NR composites.

Acknowledgement The authors would like to acknowledge the University Grants Commission and the Department of Atomic Energy Consortium, India, for the financial support.

References

1. Ponnamma D, Maria HJ, Chandra AK, Thomas S (2013) Rubber nanocomposites: latest trends and concepts. Adv Struct Mater 12:69–107
2. Harris J, Stevenson A (2011) On the role of nonlinearity in the dynamic behavior of rubber components. Rubber Chem Technol 59:740–764

3. Angellier H, Molina-Boisseau S, Dufresne A (2005) Mechanical properties of waxy maize starch nanocrystal reinforced natural rubber. Macromolecules 38:9161–9170
4. Sato S, Honda Y, Kuwahara M, Kishimoto H, Yagi N, Muraoka K, Watanabe T (2004) Microbial scission of sulfide linkages in vulcanized natural rubber by a white rot basidiomycete, ceriporiopsis s ubvermispora. Biomacromolecules 5:511–515
5. Sanguansap K, Suteewong T, Saendee P, Buranabunya U, Tangboriboonrat P (2005) Composite natural rubber based latex particles: a novel approach. Polymer 46:1373–1378
6. Ponnamma D, Sung SH, Hong JS, Ahn KH, Varughese KT, Thomas S (2014) Influence of non-covalent functionalization of carbon nanotubes on the rheological behavior of natural rubber latex nanocomposites. Eur Polymer J 53:147–159
7. Trabelsi S, Albouy PA, Rault J (2003) Effective local deformation in stretched filled rubber. Macromolecules 36:9093–9099
8. Rault J, Marchal J, Judeinstein P, Albouy PA (2006) Stress-induced crystallization and reinforcement in filled natural rubbers: 2H NMR study. Macromolecules 39:8356–8368
9. Poompradub S, Tosaka M, Kohjiya S, Ikeda Y, Toki S, Sics I, Hsiao BS (2005) Mechanism of strain-induced crystallization in filled and unfilled natural rubber vulcanizates. J Appl Phy 97:103529/1–103529/9
10. Ozbas B, Toki S, Hsiao BS, Chu B, Register RA, Aksay IA, Prud'homme RK, Adamson DH (2012) Strain-induced crystallization and mechanical properties of functionalized graphene sheet-filled natural rubber. J Polym Sci Part B Polym Phys 50:718–723
11. Brydson JA (1988) Rubbery materials and their compounds. Elsevier, Essex
12. Bode HB, Kerkhoff K, Jendrossek D (2001) Bacterial degradation of natural and synthetic rubber. Biomacromolecules 2:295–303
13. Schwerin M, Walsh D, Richardson D, Kisielewski R, Kotz R, Routson L, Lytle CD (2002) Biaxial flex-fatigue and viral penetration of natural rubber latex gloves before and after artificial aging. J Biomed Mater Res 63:739–745
14. Walsh DL, Schwerin MR, Kisielewski RW, Kotz RM, Chaput MP, Varney GW, To TM (2004) Abrasion resistance of medical glove materials. J Biomed Mater Res B 68:81–87
15. Kurian JK, Peethambaran NR, Mary KC, Kuriakose B (2000) Effect of vulcanization systems and antioxidants on discoloration and degradation of natural rubber latex thread under UV radiation. J Appl Polym Sci 78:304–310
16. Abad L, Relleve L, Aranilla C, Aliganga A, Diego CS, Rosa AD (2002) Natural antioxidants for radiation vulcanization of natural rubber latex. Polym Degrad Stab 76:275–279
17. Wu YP, Wang YQ, Zhang HF, Wang YZ, Yu DS, Zhang LQ, Yang J (2005) Rubber–pristine clay nanocomposites prepared by co-coagulating rubber latex and clay aqueous suspension. Compos Sci Technol 65(7):1195–1202
18. David JK, Hull TR (2012) A review of candidate fire retardants for polyisoprene. Polym Degrad Stab 97:201–213
19. Busfield JJC, Deeprasertkul C, Thomas AG (2000) The effect of liquids on the dynamic properties of carbon black filled natural rubber as a function of pre-strain. Polymer 41:9219–9225
20. Cai HH, Li SD, Rian TG, Wang HB, Wang JH (2003) Reinforcement of natural rubber latex film by ultrafine calcium carbonate. J Appl Polym Sci 87:982–985
21. Arroyo M, Lopez-Manchado MA, Herrero B (2003) Organo-montmorillonite as of carbon black in natural rubber compounds. Polymer 44:2447–2453
22. Jose L, Joseph R (1993) Study of the effect of polyethylene-glycol in field natural-rubber latex vulcanizates. Kaut Gummi Kunstst 46:220–222
23. Afiq MM, Azura AR (2013) Effect of sago starch loadings on soil decomposition of natural rubber latex. Int Biodeter Biodegrad 85:139–149
24. Kong LX, Peng Z, Li SD, Bartold PM (2000) Nanotechnology and its role in the management of periodontal diseases. Periodontol 40:184–196
25. Ranimol S, Thomas S (2010) Nanocomposites: state of the art, new challenges and opportunities In: Ranimol S, Thomas S (eds) Rubber nanocomposites: preparation, properties, and applications. Wiley, Singapore

26. Dufresne A (2010) Natural rubber green nanocomposites In: Ranimol S, Thomas S (eds) Rubber nanocomposites: preparation, properties, and applications. Wiley, Singapore
27. Ajayan PM, Schadler LS, Giannaris C, Rubio A (2000) Single-walled carbon nanotube–polymer composites: strength and weakness. Adv Mater 12:750–753
28. Thostenson ET (2001) Advances in the science and technology of carbon nanotubes and their composites: a review. Compos Sci Technol 61:1899–1912
29. Sadasivuni KK, Ponnamma D, Thomas S, Grohens Y (2014) Evolution from graphite to graphene elastomer composites. Prog Polym Sci 39:749–780
30. Novoselov KS (2004) Electric field effect in atomically thin carbon films. Science 306:666–669
31. Sadasivuni KK, Saiter A, Gautier N, Thomas S, Grohens Y (2013) Effect of molecular interactions on the performance of poly (isobutylene-co-isoprene)/graphene and clay nanocomposites. Colloid Polym Sci 291:1729–1740
32. Allen MJ, Tung VC, Kaner RB (2010) Honeycomb carbon: a review of graphene. Chem Rev 110:132–145
33. Zhu Y, Murali S, Cai W, Li X, Suk JW, Potts JR, Ruoff RS (2010) Graphene and graphene oxide: synthesis, properties, and applications. Adv Mater 22:3906–3924
34. Compton OC, Nguyen ST (2010) Graphene oxide, highly reduced graphene oxide, and graphene: versatile building blocks for carbon-based materials. Small 6:711–723
35. Mukhopadhyay P, Gupta RK (2011) Trends and frontiers in graphene-based polymer nanocomposites. Plast Eng 32:32–42
36. Prud'Homme RK, Ozbas B, Aksay I, Register R, Adamson D (2010) Functional graphene-rubber nanocomposites. US Patent No 7745528
37. Varghese S, Karger-Kocsis J (2004) Melt-compounded natural rubber nanocomposites with pristine and organophilic layered silicates of natural and synthetic origin. J Appl Polym Sci 91:813–819
38. Varghese S, Karger-Kocsis J (2003) Natural rubber-based nanocomposites by latex compounding with layered silicates. Polymer 44:4921–4927
39. Hambir S, Bulakh N, Jog JP (2002) Polypropylene/clay nanocomposites: effect of compatibilizer on the thermal, crystallization and dynamic mechanical behavior. Polym Eng Sci 42:1800–1807
40. Kodgire P, Kalgoannkar R, Hambir S, Bulukh N, Jog JP (2001) PP/clay nanocomposites: effect of clay treatment on morphology and dynamic mechanical properties. J Appl Polym Sci 81:1786–1792
41. Sadasivuni KK, Castro M, Saiter A, Delbreilh L, Feller JF, Thomas S, Grohens Y (2013) Development of poly(isobutylene-co-isoprene)/reduced graphene oxide nanocomposites for barrier, dielectric and sensing applications. Mater Lett 96:109–112
42. Ponnamma D, Sadasivuni KK, Grohens Y, Guo Q, Thomas S (2014) Carbon nanotubes based elastomer composites-an approach towards multifunctional materials. doi: 10.1039/C4TC01037J
43. Lin N, Yu J, Chang PR, Li J, Huang J (2011) Poly (butylene succinate)-based biocomposites filled with polysaccharide nanocrystals: structure and properties. Polym Compos 32:472–482
44. Carretero-Gonzalez J, Verdejo R, Toki S, Hsiao BS, Giannelis EP, López-Manchado MA (2008) Real time crystallization of organoclay nanoparticles filled natural rubber under stretching. Macromolecules 41:2295–2298
45. Carretero-González J, Retsos H, Verdejo R, Toki S, Hsiao BS, Giannelis EP, López-Manchado MA (2008) Effect of nanoclay on natural rubber microstructure. Macromolecules 41:6763–6772
46. Qu L, Huang G, Liu Z, Zhang P, Weng G, Nie Y (2009) Remarkable reinforcement of natural rubber by deformation-induced crystallization in the presence of organophilic montmorillonite. Acta Mater 57:5053–5060

47. Nie YJ, Huang GS, Qu LL, Wang XA, Weng GS, Wu JR (2011) New insights into thermodynamic description of strain-induced crystallization of peroxide cross-linked natural rubber filled with clay by tube model. Polymer 52:3234–3242
48. Nie YJ, Huang G, Qu L, Zhang P, Weng G, Wu JR (2011) Structural evolution during uniaxial deformation of natural rubber reinforced with nano-alumina. Adv Technol 22:2001–2008
49. Jiang HX, Ni QQ, Natsuki T (2010) Tensile properties and reinforcement mechanisms of natural rubber/vapor-grown carbon nanofiber composite. Polym Compos 31:1099–1104
50. Angles MN, Dufresne A (2000) Plasticized starch/tunicin whiskers nanocomposites 1 structural analysis. Macromolecules 33:8344–8353
51. Kim JT, Oh TS, Lee DH (2004) Curing and barrier properties of NBR/organo–clay nanocomposite. Polym Int 53:406–411
52. Putaux JL, Molina-Boisseau S, Momaur T, Dufresne A (2003) Platelet nanocrystals resulting from the disruption of waxy maize starch granules by acid hydrolysis. Biomacromolecules 4:1198–1202
53. Youssef H, Lucian AL, Orlando JR (2010) Cellulose nanocrystals: chemistry, self-assembly, and applications. Chem Rev 110:3479–3500
54. Abraham E, Deepa B, Pothan LA, Jacob M, Thomas S, Cvelbar U, Anandjiwala R (2011) Extraction of nanocellulose fibrils from lignocellulosic fibres: a novel approach. Carbohydr Polym 86:1468–1475
55. Schurz J (1999) Trends in polymer science—a bright future for cellulose. Prog Polym Sci 24:481–483
56. Teh PL, Ishak ZAM, Hashim AS, Karger-Kocsis J, Ishiaku US (2004) Effects of epoxidized natural rubber as a compatibilizer in melt compounded natural rubber–organoclay nanocomposites. Eur Polym J 40:2513–2521
57. Magaraphan R, Thaijaroen W, Lim-Ochakun R (2003) Structure and properties of natural rubber and mont morrilonite nanocomposites. Rubber Chem Technol 76:406–418
58. Nair KG, Dufresne A (2003) Crab shell chitin whisker reinforced natural rubber nanocomposites 1 processing and swelling behavior. Biomacromolecules 4:657–665
59. Nair KG, Dufresne A (2003) Crab shell chitin whisker reinforced natural rubber nanocomposites 2 mechanical behavior. Biomacromolecules 4:666–674
60. Nair KG, Dufresne A (2003) Crab shell chitin whiskers reinforced natural rubber nanocomposites 3 effect of chemical modification of chitin whiskers. Biomacromolecules 4:1835–1842
61. Peng Z, Kong LX, Li SD (2005) Non-isothermal crystallisation kinetics of self-assembled polyvinylalcohol/silica nano-composite. Polymer 46:1949–1955
62. Peng Z, Kong LX, Li SD (2005) Thermal properties and morphology of a poly (vinyl alcohol)/silica nanocomposite prepared with a self-assembled monolayer technique. J Appl Polym Sci 96:1436–1442
63. Peng Z, Kong LX, Li SD, Spiridonov P (2006) Poly (vinyl alcohol)/silica nanocomposites: morphology and thermal degradation kinetics. J Nanosci Nanotechnol 6:3934–3938
64. Li SD, Peng Z, Kong LX, Zhong JP (2006) Thermal degradation kinetics and morphology of natural rubber/silica nanocomposites. J Nanosci Nanotechnol 6:541–546
65. Saito R, Dresselhaus G, Dresselhaus MS (1998) Physical properties of carbon nanotubes. London Imperial College Press, London
66. Huczko A (2002) Synthesis of aligned carbon nanotubes. Appl Phys A Mater Sci Process 74:617–638
67. Berber S, Kwon YK, Tomanek D (2000) Unusually high thermal conductivity of carbon nanotubes. Phys Rev Lett 84:4613–4616
68. Ponnamma D, Sadasivuni KK, Strankowski M, Guo Q, Thomas S (2013) Synergistic effect of multi walled carbon nanotubes and reduced graphene oxides in natural rubber for sensing application. Soft Matter 9:10343
69. Hone J, Llaguno MC, Nemes NM, Johnson AT, Fischer JE, Walters DA, Casavant MJ, Schmidt J, Smalley RE (2000) Electrical and thermal transport properties of magnetically aligned single wall carbon nanotube films. Appl Phys Lett 77:666–668

70. Thomas PS, Abdullateef AA, Al-Harthi MA, Atieh MA, De SK, Rahaman M, Chaki TK, Khastgir D, Bandyopadhyay S (2012) Electrical properties of natural rubber nanocomposites: effect of 1-octadecanol functionalization of carbon nanotubes. J Mater Sci 47(7):3344–3349
71. Weng GS, Huang GS, Qu LL, Nie YJ, Wu JR (2010) Large-scale orientation in a vulcanized stretched natural rubber network: proved by in situ synchrotron X-ray diffraction characterization. J Phys Chem B 114:7179–7188
72. Tonpheng B, Andersson O (2008) Crosslinking, thermal properties and relaxation behaviour of polyisoprene under high-pressure. Eur Polym J 44:2865–2873
73. Liang J, Huang Y, Ma Y, Liu Z, Cai J, Zhang C, Gao H, Chen Y (2009) Electromagnetic interference shielding of graphene/epoxy composites. Carbon 47:922–925
74. De Rosa M, Mancinelli R, Sarasini F, Sarto MS, Tamburrano A (2009) Electromagnetic design and realization of innovative fiber-reinforced broad-band absorbing screens. IEEE Trans Electromag Compat 51:700–707
75. De Rosa M, Dinescu A, Sarasini F, Sarto MS, Tamburrano A (2010) Effect of short carbon fibers and MWCNTs on microwave absorbing properties of polyester composites containing nickel coated carbon fibers. Compos Sci Technol 70:102
76. De Bellis G, De Rosa IM, Dinescu A, Sarto MS, Tamburrano A (2010) Proceedings of the 2010 IEEE international symposium on electromagnetic compatibility, Fort Lauderdale 202
77. Angellier H, Molina-Boisseau S, Belgacem MN, Dufresne A (2005) Surface chemical modification of waxy maize starch nanocrystals. Langmuir 21:2425–2433
78. Trovatti E, Carvalho AJF, Ribeiro SJL, Gandini A (2013) Simple green approach to reinforce natural rubber with bacterial cellulose nanofibers. Biomacromolecules 14(8):2667–2674
79. Avérous L, Halley PJ (2009) Biocomposites based on plasticized starch. Biofuels Bioprod Bioref 3:329
80. Avérous L (2004) Biodegradable multiphase systems based on plasticized starch: a review. J Macromol Sci C Polym Rev C 44:231–274
81. Ray S, Bousmia M (2005) Biodegradable polymers and their layered silicate nanocomposites: in greening the 21st century materials world. Prog Mater Sci 50:962–1079
82. Roy N, Sengupta R, Bhowmick AK (2012) Modifications of carbon for polymer composites and nanocomposites. Prog Polym Sci 37(6):781–819
83. Dufresne A, Cavaille JY, Helbert W (1996) New nanocomposite materials: microcrystalline starch reinforced thermoplastic. Macromolecules 29:7624–7626
84. Baek JB, Lyons CB, Tan LS (2004) Grafting of vapor-grown carbon nanofibers via in-situ polycondensation of 3-phenoxybenzoic acid in poly (phosphoric acid). Macromolecules 37:8278–8285
85. Lu YL, Ye FY, Mao LX, Li Y, Zhang LQ (2011) Micro-structural evolution of rubber/clay nanocomposites with vulcanization process. Express Polym Lett 5:777–787
86. Coleman JN, Khan U, Blau WJ, Gunko YK (2006) Small but strong: a review of the mechanical properties of carbon nanotube–polymer composites. Carbon 44:1624–1652
87. Du JH, Bai J, Cheng HM (2007) The present status and key problems of carbon nanotube based polymer composites. eXPRESS Polym Lett 1:253–273
88. Jiang C, He H, Jiang H, Ma L, Jia D M (2013) Nano-lignin filled natural rubber composites: preparation and characterization. eXPRESS Polym Lett 7:480–493
89. Majdzadeh-Ardakani K, Ardakani Sh Sadeghi- (2010) Experimental investigation of mechanical properties of starch/natural rubber/clay nanocomposites. Digest J Nanomater Biostructures 5:307–316
90. Lopez-Manchado MA, Herrero B, Arroyo M (2003) Preparation and characterization of organoclay nanocomposites based on natural rubber. Polym Int 52:1070–1077
91. Andrews R, Jacques D, Minot M, Rantell T (2002) Fabrication of carbon multiwall nanotube/polymer composites by shear mixing. Macromol Mater Eng 287:395–403

92. Breuer O, Sundararaj U (2004) Big returns from small fibers: a review of polymer/carbon nanotube composites. Polym Compos 25:630–645
93. Liu Q, Zhang D, Fan T, Gu J, Miyamoto Y, Chen Z (2008) Amorphous carbon-matrix composites with interconnected carbon nano-ribbon networks for electromagnetic interference shielding. Carbon 46(3):461–465
94. Zhang CS, Ni QQ, Fu SY, Kurashiki K (2007) Electromagnetic interference shielding effect of nanocomposites with carbon nanotube and shape memory polymer. Compos Sci Technol 67:2973–2980
95. Yakuphanoglu F, Al-Ghamdi AA, El-Tantawy F (2014) Electromagnetic interference shielding properties of nanocomposites for commercial electronic devices. Microsyst Technol 1–9
96. Tanrattanakul V, Bunchuay A (2007) Microwave absorbing rubber composites containing carbon black and aluminum powder. J Appl Polym Sci 105:2036–2045
97. Kong I, Ahmada S, Abdullah MH, Hui D, Yusoff AN, Puryanti D (2010) Magnetic and microwave absorbing properties of magnetite-thermoplastic natural rubber nanocomposites. J Mag Mag Mater 322:3401–3409
98. Al-Hartomy OA, Al-Ghamdi A, Dishovsky N, Shtarkova R, Iliev V, Mutlay I, El-Tantawy F (2012) Dielectric and microwave properties of natural rubber based nanocomposites containing graphene. Mater Sci Appl 3:453
99. Arief PT, Kean CA, Jadranka T (2012) A novel polypyrrole and natural rubber based flexible large strain sensor. Sens Actuators B 20:166
100. He Q, Yuan T, Zhang X, Guo S, Liu J, Liu J, Liu X, Sun L, Wei S, Guo Z (2014) Heavy duty piezoresistivity induced strain sensing natural rubber/carbon black nanocomposites reinforced with different carbon nanofillers. Mater Res Express 1(3):035029
101. Tadakaluru S, Thongsuwan W, Singjai P (2014) Stretchable and flexible high-strain sensors made using carbon nanotubes and graphite films on natural rubber. Sensors 14:868–876
102. Knite M, Tupureina V, Fuith A, Zavickis J, Teteris V (2007) Polyisoprene—multi-wall carbon nanotube composites for sensing strain. Mater Sci Eng C 27:1125
103. Herculano RD, Brunello CA, Graeff CFO (2007) Optimization of a novel nitric oxide sensor using a latex rubber. J Appl Sci 7:3801
104. John H, Joseph R, Mathew KT (2007) Dielectric behavior of natural rubber composites in microwave fields. J Appl Polym Sci 103:2682–2686
105. Makled HM (2012) Dielectric properties of high coercivity barium ferrite–natural rubber composites. J Appl Polym Sci 126:969
106. Haseena AP, Unnikrishnan G, Kalaprasad G (2007) Dielectric properties of short sisal/coir hybrid fibre reinforced natural rubber composites. Compos Interf 14:763–786
107. Popielarz R, Chiang CK, Nozaki R, Obrzut J (2001) Dielectric properties of polymer/ferroelectric ceramic composites from 100 Hz to 10 GHz. Macromolecules 34:5910–5915
108. Marzinotto M, Santulli C, Mazzetti C (2007) Dielectric properties of oil palm-natural rubber biocomposites. IEEE Electr Insul Dielectr Phenom CEIDP 9777934:584–587
109. Jacob M, Varughese KT, Thomas S (2006) Dielectric characteristics of sisal—oil palm hybrid biofibre reinforced natural rubber biocomposites. J Mater Sci 41:5538–5547
110. Jacob M, Thomas S, Varughese KT (2004) Mechanical properties of sisal/oil palm hybrid fiber reinforced natural rubber composites. Compos Sci Tech 64:955–965
111. Tangboriboon N, Uttanawanit N, Longtong M, Wongpinthong P, Sirivat A, Kunanuruksapong R (2010) Electrical and electrorheological properties of alumina/natural rubber (STR XL). Compos Compos Mater 3:656–671
112. Elimat ZM, Zihlif AM, Ragosta G (2008) Study of ac electrical properties of aluminium–epoxy composites. J Phys D Appl Phys 41:165408
113. Musameh SM, Abdelazeez MK, Ahmad MS, Zihlif AM, Malinconico M, Martuscelli E, Ragosta G (1991) Some electrical properties of aluminum-epoxy composite. Mater Sci Eng B 10:29–33
114. Sadasivuni KK, Ponnamma D, Kumar B, Strankowski M, Cardinaels R, Moldenaers P, Thomas S, Grohens Y (2014) Dielectric properties of modified graphene oxide filled

polyurethane nanocomposites and its correlation with rheology. Compos Sci Technol 104:18–25
115. Dang ZM, Nan CW, Xie D, Zhang YH, Tjong SC (2004) Dielectric behavior and dependence of percolation threshold on the conductivity of fillers in polymer-semiconductor composites. Appl Phys Lett 85:97–99
116. Sinclair DC, Adams TB, Morrison FD, West AR (2002) CaCu3Ti4O12: one-step internal barrier layer capacitor. Appl Phys Lett 80:2153–2155
117. Jana PK, Sarkar S, Sakata H, Watanabe T, Chaudhuri BK (2008) Microstructure and dielectric properties of NaxTiyNi1 − x−yO (x = 0.05–0.30, y = 0.02). J Phys D Appl Phys 41:65403
118. Pohl HA (1978) Dielectrophoresis. Cambridge University Press, London
119. Jamal EMA, Joy PA, Kurian P, Anantharaman MR (2009) Synthesis of nickel–rubber nanocomposites and evaluation of their dielectric properties. Mater Sci Eng B 156:24–31
120. Psarras GC, Gatos KG, Karahaliou PK, Georga SN, Krontiras CA, Karger-Kocsis J (2007) Relaxation phenomena in rubber/layered silicate nanocomposites. eXPRESS Polym Lett 1:837–845
121. Kornev A, Bukanov A, Sheverdiaev O (2005) Technology of elastomeric materials, in Russian. Istek, Moscow
122. Banerjee P, Biswas S (2011) Dielectric properties of EVA rubber composites at microwave frequencies theory, instrumentation and measurements. J Micro Power Electromag Energ 45:24–29
123. Hernández M, Bernal MM, Verdejo R, Ezquerra TA, López-Manchado MA (2012) Overall performance of natural rubber/graphene nanocomposites. Compos Sci Technol 73:40–46
124. Yu J, Andersson O (2009) Thermal conductivity, heat capacity, and cross-linking of polyisoprene/single-wall carbon nanotube composites under high pressure. Macromolecules 42:9295–9301
125. Wei C, Srivastava D, Cho K (2002) Thermal expansion and diffusion coefficients of carbon nanotube-polymer composite. Nano Lett 2:647–650
126. Flaifel MH, Ahmad SH, Hassan A, Bahri S, Tarawneh MA, Yu L (2013) Thermal conductivity and dynamic mechanical analysis of NiZn ferrite nanoparticles filled thermoplastic natural rubber nanocomposites. Compos Part B 52:334–339
127. Gojny FH, Wichmann MHG, Fiedler B, Kinloch IA, Bauhofer W, Windle AH, Schulte K (2006) Evaluation and identification of electrical and thermal conduction mechanisms in carbon nanotube/epoxy composites. Polymer 47:2036–2045
128. Potts JR, Shankar O, Du L, Ruoff RS (2012) Processing–morphology–property relationships and composite theory analysis of reduced graphene oxide/natural rubber nanocomposites. Macromolecules 45:6045–6055
129. Zakaria MZ, Ahmad SH (2013) Investigation on thermal conductivity and mechanical properties of thermoplastic natural rubber filled with alumina and boron carbide nanocomposites. Energ Environ Eng J 2:11–14
130. Zhan Y, Wu J, Xia H, Yan N, Fei G, Yuan G (2011) Dispersion and exfoliation of graphene in rubber by an ultrasonically-assisted latex mixing and in situ reduction process. Macromol Mater Eng 296:590–602
131. Meera AP, Tlili R, Boudenne A, Ibos L, Poornima V, Thomas S, Candau Y (2012) Thermophysical and mechanical properties of TiO_2 and silica nanoparticle-filled natural rubber composites. J Elast Plast 44:1–14
132. Zhamu A, Bor JZ (2011) Pristine nano graphene-modified tyres. US Patent 2011/0046289A1
133. Ponnamma D, Sadasivuni KK, Strankowski M, Moldenaers P, Thomas S, Grohens Y (2013) Interrelated shape memory and Payne effect in polyurethane/graphene oxide nanocomposites. RSC Adv 3:16068
134. Fukahori Y (2010) Mechanism of the self-reinforcement of cross-linked NR generated through the strain-induced crystallization. Polymer 51:1621–1631

135. Heuwers B, Quitmann D, Hoeher R, Reinders FM, Tiemeyer S, Sternemann C, Tolan M, Katzenberg F, Tiller JC (2013) Stress-induced stabilization of crystals in shape memory natural rubber. Macromol Rapid Commun 34:180–184
136. Katzenberg F, Heuwers B, Tiller JC (2011) Superheated rubber for cold storage. Adv Mater 23:1909–1911
137. Heuwers B, Beckel A, Krieger A, Katzenberg F, Tiller JC (2013) Shape-memory natural rubber: an exceptional material for strain and energy storage. Macromol Chem Phys 214:912
138. Bruns N, Tiller JC (2006) Nanophasic amphiphilic conetworks with a fluorophilic phase. Macromolecules 39:4386
139. Quitmann D, Gushterov N, Sadowski G, Katzenberg F, Tiller JC (2013) Solvent-sensitive reversible stress-response of shape memory natural rubber. ACS Appl Mater Interf 5:3504
140. Jincheng W, Yan G (2011) Hyperbranched intumescent flame-retardant agent: application to natural rubber composites. J Appl Polym Sci 122:3474
141. Niamlang S, Thongchai S, Pawananant N, Sirivat A (2013) The electromechanical properties of crosslinked natural rubber. Energy Procedia 34:697–704
142. Puvanatvattana T, Chotpattananont D, Hiamtup P, Niamlang S, Sirivat A, Jamieson AM (2006) Electric field induced stress moduli in polythiophene/polyisoprene elastomer blends. React Funct Polym 66:1575–1588
143. Sirivat A, Petcharoen K, Pornchaisiriarun Y, Phansa-Ard C, Tangboriboon N (2014) Lead zirconate (PbZrO3) embedded in natural rubber as electroactive elastomer composites. J Innovative Opt Health Sci 7:1450016
144. Tangboriboon N, Datsanae S, Onthong A, Kunanuruksapong R, Sirivat A (2012) Electromechanical responses of dielectric elastomer composite actuators based on natural rubber and alumina. J Elastomers Plast 45:143–161
145. Niamlang S, Thongchai S, Pawananant N, Sirivat A (2013) The electromechanical properties of crosslinked natural rubber. Energy Procedia 34:697–704